



1 Influence of Ocean Alkalinity Enhancement with Olivine or Steel 2 Slag on a Coastal Plankton Community in Tasmania

3

4 Jiaying A. Guo^{1,2}, Robert F. Strzepek², Kerrie M. Swadling^{1,2}, Ashley T. Townsend³, Lennart T. Bach¹

5 ¹Institute for Marine and Antarctic Studies, University of Tasmania, Hobart, Tasmania, 7000 Australia

6 ²Australian Antarctic Program Partnership (AAPP), Institute for Marine and Antarctic Studies, University of Tasmania,
7 Hobart, Tasmania, 7000 Australia

8 ³Central Science Laboratory, University of Tasmania, Sandy Bay, Tasmania, 7005 Australia

9 Correspondence to: Jiaying A. Guo (Jiaying.guo@utas.edu.au)

10

11 **Abstract.** Ocean alkalinity enhancement (OAE) aims to increase atmospheric CO₂ sequestration in the oceans through the
12 acceleration of chemical rock weathering. This could be achieved by grinding rocks containing alkaline minerals and
13 adding the rock powder to the surface ocean where it dissolves and chemically locks CO₂ in seawater as bicarbonate.
14 However, CO₂ sequestration during dissolution coincides with the release of potentially bio-active chemicals and may
15 induce side effects. Here, we used 53 L microcosms to test how coastal plankton communities from Tasmania respond to
16 OAE with olivine (mainly Mg₂SiO₄) or steel slag (mainly CaO and Ca(OH)₂) as alkalinity sources. Three microcosms were
17 left unperturbed and served as a control, three were enriched with olivine powder (1.9 g L⁻¹), and three with steel slag
18 powder (0.038 g L⁻¹). Phytoplankton and zooplankton community responses as well as some biogeochemical parameters
19 were monitored for 21 days. Olivine and steel slag additions increased total alkalinity by 29 μmol kg⁻¹ and 361 μmol kg⁻¹
20 respectively, which corresponds to a theoretical increase of 0.9 % and 14.8 % of the seawater storage capacity for
21 atmospheric CO₂. Olivine and steel slag released silicate nutrients into the water column, but steel slag released
22 considerably more and also significant amounts of phosphate. Both minerals released dissolved aluminium (>400 nmol L⁻¹
23 ¹). The slag addition increased dissolved manganese concentrations (784 nmol L⁻¹), while olivine increased dissolved nickel
24 concentrations (38 nmol L⁻¹). The slag treatment increased the total particulate manganese concentrations (22 nmol L⁻¹),
25 while olivine increased the total particulate nickel (5 nmol L⁻¹), which was consistent with the increase in the dissolved
26 concentrations of these trace metals in seawater. There was no significant difference in total chlorophyll *a* concentrations
27 between the treatments and the control, likely due to nitrogen limitation of the phytoplankton community. However, flow
28 cytometry results indicated an increase in the cellular abundance of several smaller (<20 μm) phytoplankton groups in
29 the olivine treatment compared to the slag treatment and the control. The abundance of larger phytoplankton (>20 μm)
30 decreased much more in the control than in the mineral addition treatments after day 10. Furthermore, the maximum
31 quantum yields of photosystem II (F_v/F_m) were higher in slag and olivine treatments, suggesting that mineral additions
32 increased photosynthetic performance. The zooplankton community composition was also affected with the most notable
33 changes being observed in the dinoflagellate *Noctiluca scintillans* and the appendicularian *Oikopleura* sp. Overall, steel
34 slag is much more efficient for CO₂ removal with OAE than olivine and appears to induce less changes in the plankton
35 community when relating the CO₂ removal potential to the level of environmental impact that was observed here.

36



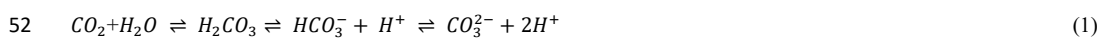
37 1 Introduction

38 Keeping global warming below 2 °C requires immediate emissions reduction. Additionally, between 450-1100 Gigatonnes
39 of carbon dioxide (CO₂) need to be removed from the atmosphere by 2100 (Smith et al., 2023). This could be achieved
40 with a portfolio of terrestrial and marine Carbon Dioxide Removal (CDR) methods. Ocean alkalinity enhancement (OAE)
41 is a marine CDR method that could theoretically contribute significantly to the global CDR portfolio (Ilyina et al., 2013;
42 Feng et al., 2017; Lenton et al., 2018).

43

44 Alkalinity is generated naturally when rock weathers and it has control on the ocean's chemical capacity to store CO₂
45 (Schuiling and Krijgsman, 2006). Natural rock weathering is currently responsible for about 0.5 Gt of atmospheric CO₂
46 sequestration every year (Renforth and Henderson, 2017). The idea behind OAE is to accelerate natural rock weathering
47 by extracting calcium- or magnesium-rich rocks, such as olivine, pulverizing them, and spreading them onto the sea surface
48 to increase chemical weathering rates (Hartmann et al., 2013). The weathering (i.e., dissolution) of these alkaline minerals
49 will consume protons (H⁺), which shifts the carbonate chemistry equilibrium in seawater from CO₂ towards increasing
50 bicarbonate (HCO₃⁻) and carbonate ion (CO₃²⁻) concentrations:

51



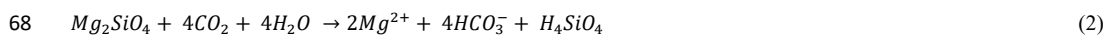
53

54 thereby making new space for atmospheric CO₂ to be dissolved in seawater and permanently stored. Previous model studies
55 have shown that OAE can mitigate climate change significantly by increasing the oceanic uptake of CO₂ from the
56 atmosphere (Kohler et al., 2010; Paquay and Zeebe, 2013; Keller et al., 2014; Lenton et al., 2018). For example, the study
57 by Burt et al. (2021) suggested that the total global mean dissolved inorganic carbon (DIC) inventories would increase by
58 156 GtC after total alkalinity is enhanced at a rate of 0.25 Pmol year⁻¹ in 75-year simulations.

59

60 There are a variety of alkaline minerals that could be used for OAE. A widely considered naturally occurring mineral is
61 forsterite, a (Mg₂SiO₄)-rich olivine. This type of olivine is abundant in ultramafic rock such as dunite, constituting at least
62 88 % of the rock composition (Ackerman et al., 2009; Su et al., 2016). Olivine occurs in the Earth's crust but is more
63 abundant in the upper mantle. There are at least several billion tons of olivine resources on Earth (Caserini et al., 2022).
64 However, the extraction of olivine in 2017 was only around 8.4 Mt year⁻¹ (Reichl et al., 2018), which is about two orders
65 of magnitude below the mass needed for climate-relevant OAE with olivine (Caserini et al., 2022). The net reaction for
66 CO₂ sequestration with Mg₂SiO₄ is:

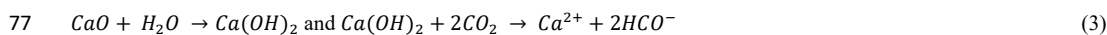
67



69

70 Another potential OAE source material is steel slag (Renforth, 2019), a by-product of steel manufacturing. During steel
71 manufacturing, high-purity calcium oxide (CaO) is used to improve the quality of the steel through accumulation of
72 unwanted materials such as sulphur and phosphorus. Steel slag mainly contains CaO, SiO₂, Al₂O₃, Fe₂O₃, MgO, and MnO
73 (Kourounis et al., 2007), and the chemical composition can vary depending on the manufacturing process (Wang et al.,
74 2011). Due to the presence of CaO and potentially other alkaline components, steel slag can increase alkalinity when
75 dissolved in seawater. The chemical reaction for CO₂ sequestration with CaO is:

76



78

79 Some of the steel slag that is produced during steel manufacturing is further used (e.g. for road construction and civil
80 engineering) but in some countries like China, 70.5 % of steel slag is left unused and stored in dumps (Guo et al., 2018).
81 In 2016, more than 300 million tons of steel slag was not used effectively, thereby occupying the land and raising
82 environmental concerns (Guo et al., 2018). The effective alkaline composition, availability, and relatively low cost of the
83 raw materials make olivine and steel slag potential source materials for OAE.

84

85 To assess whether OAE is viable, it needs to be understood how its application may affect marine biota such as plankton
86 and the biogeochemical fluxes they drive. Some data on the effects of OAE with sodium hydroxide (NaOH) on plankton
87 communities have recently been published (Ferderer et al., 2022; Subhas et al., 2022), but to the best of our knowledge, no
88 such data is available for olivine- and/or slag-based OAE. Chemical perturbations via olivine and slag should be like those
89 by NaOH in that they increase seawater pH and shift the carbonate chemistry equilibrium (see Eq. 1). However, there
90 would be additional chemical perturbations because minerals contain a variety of potentially bioactive elements that are
91 released into the environment when they dissolve in seawater (Bach et al., 2019). One particular concern is that natural and
92 anthropogenic minerals such as olivine and steel slag are rich in bioactive metals that are usually scarce in the ocean, such
93 as iron (Fe), copper (Cu), nickel (Ni), manganese (Mn), zinc (Zn), cadmium (Cd), and chromium (Cr). Many of these trace
94 metals are essential micronutrients for phytoplankton growth (Sunda, 2000; Sunda, 2012), such as being co-factors for
95 various metalloenzymes (summarized by Twining and Baines (2013)). It is possible that the addition of alkaline minerals
96 may benefit phytoplankton by providing trace metals currently limiting phytoplankton growth (Falkowski, 1994; Basu and
97 Mackey, 2018). For instance, the addition of Fe is well known to stimulate phytoplankton blooms in those vast ocean
98 regions where Fe levels limit growth (Boyd et al., 2007; Moore et al., 2013). However, some trace metals can also inhibit
99 phytoplankton growth, and different phytoplankton species have different requirements and tolerances for trace metals
100 (Sunda, 2012) so the addition of trace metals via OAE may change the plankton community composition.

101

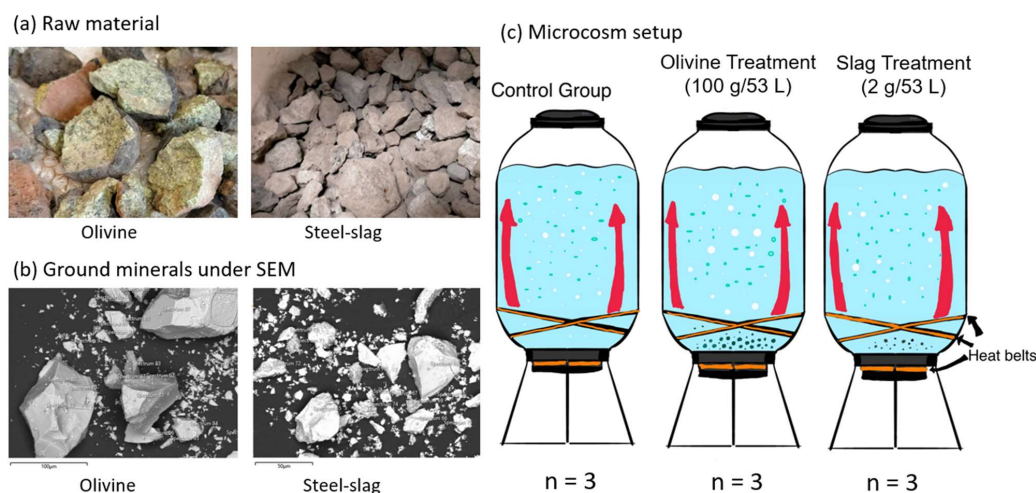
102 Here, we describe a microcosm experiment with coastal Tasmanian plankton communities that was used to investigate: (1)
103 how effectively OAE via the application of finely ground olivine and steel-slag could sequester atmospheric CO₂, and (2)
104 if/how olivine and steel-slag additions affect various components of the plankton community.

105



106 **2 Methodology**

107 **2.1 Microcosm setup**



108 **Fig. 1.** Experimental design and alkalinity sources. (a) Raw materials used as alkalinity sources: olivine (left) and steel-slag (right).
109 Olivine and steel-slag were originally larger than 20 mm. (b) Ground minerals observed with a scanning electron microscope. (c)
110 Microcosm setup: each microcosm enclosed ~ 53 L of surface seawater with natural plankton communities. Olivine and steel-slag
111 treatments and the control were kept in a temperature-controlled room and two heat belts were attached to the bottom of each microcosm
112 to create convective circulation.
113

114

115 We used nine 53 L transparent Kegland® Fermzilla conical unitank fermenters (polyethylene terephthalate) (Fig. 1) as
116 microcosms to incubate natural plankton communities. All microcosms were prewashed with hydrochloric acid (10 % v/v)
117 and rinsed five times with 18.2 MΩ Milli-Q water. Seawater with coastal plankton communities was collected at Battery
118 Point, Tasmania (42.892°S, 147.337°E) within 2 hours by lowering the microcosms into the ocean with a crane and filling
119 them in a manner similar to a Niskin bottle, as described in detail in Ferderer et al. (2022). A sieve with a mesh size of 2
120 mm was attached to the top and bottom of the microcosms during filling to avoid the entrapment of large and patchily
121 distributed organisms in the microcosms. The enclosed seawater weight was initially between 52.35-54.70 kg. After
122 seawater collection, filled microcosms were immediately transported back to the Institute for Marine and Antarctic Studies
123 (University of Tasmania) on a truck and transferred within 75 min into a temperature-controlled room set to 7.5-8 °C. Two
124 heat belts were attached to the bottom of each microcosm to induce a convective mixing current (Ferderer et al., 2022).
125 Seawater temperature inside the microcosms was about 13.5 °C due to the heating effects of the heat belts, and was the
126 same as the sampled region. LED light strips were used to provide an average light intensity of 236 $\mu\text{mol photons m}^{-2} \text{ s}^{-1}$
127 (ranging from 208 to 267 $\mu\text{mol photons m}^{-2} \text{ s}^{-1}$) with a daily light-dark cycle of 10:14 hours. The light intensity was the
128 average light intensity in each microcosm measured with a LICOR light meter at 0.15 m depth within the microcosm.
129 Microcosms positioned in the temperature-controlled room were shuffled anti-clockwise every day to ensure similar light
130 intensity for each microcosm throughout the experiment. Treatments were established 24 hours after collecting the seawater.
131 The total alkalinity released per amount of mineral powder added was much higher for the slag powder than the olivine



132 powder in our preliminary test trials. So, three microcosms were enriched with 100 g of olivine powder, three microcosms
133 with 2 g of steel slag powder, while the remaining three microcosms were left unperturbed and served as controls.
134

135 **2.2 Preparation of olivine and steel slag powder**

136 The olivine rocks were provided by Moyne Shire Council who sourced the mineral from a quarry in Mortlake, Victoria,
137 Australia. The Basic Oxygen Slag (hereafter referred to as “slag”) was provided by Bradley Mansell who sourced the
138 material from Liberty Primary Steel Whyalla Steelworks in Whyalla, South Australia, Australia. Upon delivery, the olivine
139 rocks were 40-80 mm in diameter, and slag aggregates were 20-50 mm in diameter. These were crushed to smaller than 10
140 mm pieces using a hydraulic crusher. The crushed material was further ground with a ring mill with a chrome milling pot.
141 Afterwards, finely-ground samples were sieved to get samples with 150 ~ 250 μm grain size. The sieved olivine and slag
142 grains were inspected for their appearance and elemental composition using a Hitachi SU-70 analytical field emission
143 scanning electron microscope (SEM), and energy dispersive spectrometers (Central Science Laboratory (CSL), University
144 of Tasmania). Grain size spectra were determined with a Sympatec QICPIC particle size analyser LIXCELL (CSL,
145 University of Tasmania).
146

147 **2.3 Seawater sampling**

148 Seawater was transferred with a peristaltic pump from the microcosms at a depth of about 0.15 m into 1 L acid-washed
149 sampling bottles (LDPE) using an acid-washed silicon tube. Seawater in these bottles was then subsampled for dissolved
150 trace metal samples, filtrations, Fast Repetition Rate fluorometry (FRRf), and flow cytometry analysis. Samples for
151 nutrients and total alkalinity (TA) were transferred using the same pump but through a silicone tube into 80 mL HDPE
152 bottles. Total alkalinity and macronutrient samples were filtered during this process through a 0.2 μm nylon filter attached
153 to the silicone tube to remove all particles and organisms $> 0.2 \mu\text{m}$.
154

155 **2.4 Salinity, nutrients, carbonate chemistry, and trace metal analysis**

156 Salinity was measured before and at the end of the experiment using a HACH HQ40d portable meter. The pH_T (total scale)
157 and temperatures were measured daily (2-3 hours after the onset of the light period) using a pH meter (914
158 pH/Conductometer Metrohm). We recorded voltages and temperature from the pH meter and calibrated the pH_T at original
159 temperature at sampled time using the certified reference material (CRM) Tris buffer following the method described in
160 SOP6a by Dickson et al. (2007). Briefly, the standard buffer’s pH and voltage at different temperature gradients were
161 recorded, and temperature vs. voltage polynomial regression data were generated for calculating calibrated pH values (pH_T)
162 (refer to Eq. 3 in SOP6a of Dickson et al. (2007)). The regression could then be used to obtain a CRM pH value for each
163 temperature and to calibrate the pH measured in the microcosms to the total pH scale.
164

165 Total alkalinity was sampled every four days. It was measured in duplicate using a Metrohm 862 Compact Titrosampler
166 coupled with an Aquatode Plus with PT1000 temperature sensor following the SOP3b open-cell titration protocol
167 described in Dickson et al. (2007). Filtered TA samples were stored at 8 $^{\circ}\text{C}$ for a maximum of 23 days before measurement.



168 Titration curves were evaluated using the “calculate” script within PyCO2sys by Humphreys et al. (2022). The carbon
169 chemistry equilibrium was calculated with the R package “seacarb” Gattuso et al. (2023) from pH_T, TA, phosphate, silicate,
170 temperature, and salinities using stoichiometric equilibrium constants from Lueker et al. (2000). Dissolved macronutrients
171 were measured every second day using standard spectrophotometric methods developed by Hansen and Koroleff (1999)
172 on the day the samples were taken from the microcosms.

173

174 Dissolved trace metal concentrations were measured four times during the experiment: a few hours before olivine and slag
175 were added, a few hours after these minerals were added on day 2, near the middle of the experiment on day 13, and at the
176 end of the experiment on day 22. Sixty mL of seawater was collected using an acid-washed 60 mL syringe, and the seawater
177 was filtered through 25 mm diameter 0.2 µm pore size polycarbonate filters. Unfortunately, we did not notice that 0.2 µm
178 pore size nylon filters (acid washed) were used during sampling on days 1 and 2 so we refiltered these seawater samples
179 again using 0.2 µm pore size polycarbonate filters after one month. All seawater samples were diluted approximately 20-
180 fold by weight using Milli-Q water (18.2 MΩ·cm grade) and acidified using 1 % ultrapure HCl. These samples were
181 analysed using Sector Field Inductively Coupled Plasma Mass Spectrometry (SF-ICP-MS) employing multiple resolution
182 settings to overcome major spectral interferences. Due to the presence of abundant major metal ions in our samples, such
183 as Na and Mg, natural open-ocean seawater from the Southern Ocean with very low trace metal concentrations was diluted
184 20 times with Milli-Q water and used as a representative blank. The same Southern Ocean seawater was enriched
185 with different gradients of trace metal standards to calculate the samples’ trace metal concentrations. Seven of the total 36
186 samples had abnormal trace metal or phosphate concentrations, and 4 of them were from day 1. We considered them as
187 contaminated using the interquartile range (IQR) criterion and excluded them from the data analysis.

188

189 **2.5 Particulate matter and plankton community analysis**

190 Chlorophyll *a* was sampled every second day by filtering the seawater through glass fibre filters (GF/F, pore size = 0.7 µm,
191 diameter = 25 mm), and filters were stored in 15 mL polypropylene tubes wrapped with aluminium foil and stored at -80 °C
192 for 50-70 days before measurement. Each filter was immersed in 10 mL 100 % methanol for 18-20 h to extract chlorophyll
193 from phytoplankton and these samples were analysed on a Turner fluorometer (Model 10-AU) following the method
194 described by Evans et al. (1987).

195

196 Phytoplankton flow cytometry samples were fixed with 40 µL of a mixture of formaldehyde-hexamine (18 %:10 % v/w)
197 added to 1400 µL of seawater sample. All bacteria samples (700 µL) were fixed with 14 µL glutaraldehyde (Electron-
198 microscope grade, 25 %). After mixing samples with fixatives, samples were stored for 25 minutes at 10 °C, then flash-
199 frozen in liquid nitrogen, and stored at -80 °C until measurement 83-86 days later. Directly before the measurement,
200 samples were thawed at 37 °C. Bacteria samples were stained with SYBR green I (diluted in dimethylsulfoxide) at a final
201 ratio of 1:10000 (SYBR Green I: sample).

202

203 A Cytex Aurora flow cytometer (Cytex Biosciences) was used to quantify the abundance of fluorescing particles such as
204 phytoplankton or stained bacteria. Phytoplankton groups were distinguished based on their fluorescence signal intensity of
205 different laser excitation/emission wavelength combinations and forward scatter (FSC). The yellow-green laser (centre
206 wavelength: 577 nm), in combination with FSC signal strength, was used to separate cyanobacteria and cryptophytes from



207 other phytoplankton. The violet laser (centre wavelength: 664 nm) in combination with FSC was used to distinguish
208 picoeukaryotes, nanoeukaryotes, and microphytoplankton. The blue laser (centre wavelength: 508 nm) in combination with
209 FSC was used to distinguish bacteria from other living (i.e., DNA-containing) particles (Fig. S. 1).

210

211 The biovolume of each classified flow cytometry phytoplankton type was calculated using the equation:

212

$$213 \text{ Biovolume} = \text{Cell number count} \times \left(\frac{\text{FSC}}{10248}\right)^{2.14} \quad (4)$$

214

215 Where biovolume is the biovolume of the phytoplankton (μm^3), cell number is the cell count per mL of sample, and the
216 FSC is the forward scatter signal value from the flow cytometry. This equation is calculated based on the relationship
217 between biovolume and FSC for different phytoplankton species (Selfe, 2022).

218

219 Phytoplankton photosynthetic performance was estimated from the rapid light curves measured with an FRRf (FastOcean
220 Sensor FRRf3, Chelsea Instruments Group) every second day following the protocol adapted from Schallenberg et al.
221 (2020). Samples were kept in the dark for 20 minutes before the measurement and then added to the FRR fluorometry
222 cuvette, which was temperature-controlled at 13.5 °C. Filtered natural seawater was used for blank correction. The channel
223 with different light wavelengths (450, 530, and 624 nm) was used in each acquisition sequence. At least 10 acquisitions
224 were measured for each sample. The maximum electron transport rate (ETR_{max}), initial slope of the rapid light curve (α),
225 and the light-saturation parameter (E_k) were calculated using the equation described by Platt et al. (1980) without
226 photoinhibition:

227

$$228 \text{ ETR} = \text{ETR}_{\text{max}} \left[1 - e^{-\frac{\alpha E}{\text{ETR}_{\text{max}}}}\right] \quad (5)$$

229

230 These parameters together with the maximum quantum yield of PSII (F_v/F_m) were used to compare the photosynthetic
231 performance of the phytoplankton communities in different microcosms.

232

233 Seawater was sampled before the treatment and at the end of the experiment for particulate trace metal concentrations.
234 Samples of 100 mL were filtered through an acid-cleaned polycarbonate filter (25 mm diameter, 0.8 μm pore size) and
235 placed in an acid-cleaned polypropylene filter holder on a trace metal-clean bench. The filters were washed with the EDTA-
236 oxalate reagent (1.4 mL) twice (8 min total) and rinsed with chelexed NaCl solution (0.6 mol L⁻¹ with 2.38 mmol L⁻¹ of
237 HCO₃⁻, pH=8.2) 10 times (1.5 mL aliquots) (Tang and Morel, 2006). Filters were stored in acid-washed well plates at -
238 20 °C before analysis. The digestion process followed the method reported by Bowie et al. (2010). Briefly, all samples and
239 triplicate certified reference materials plankton standards (50 mg/vial) were digested in a mixture of strong ultrapure acids
240 (750 μL 12 mol L⁻¹ HCl, 250 μL 40 % HF, 250 μL 14 mol L⁻¹ HNO₃) in 15 mL Teflon perfluoroalkoxy (PFA) vials on a
241 95 °C hot plate for 12 h in a fume hood. They were then dry evaporated for 4 h and re-suspended in 10 % v-v ultrapure
242 HNO₃. All prepared solutions had indium as internal standard added to a final concentration of 10 μg L⁻¹. Three pre-mixed
243 multi-element standard solutions (MISA) were prepared as external calibration standards.

244

245 Particulate organic carbon (POC) was sampled by filtering 100 mL of seawater from each microcosm. Glass fibre filters
246 (Whatman GF/F, pore size =0.7 μm , diameter =13 mm) were pre-combusted at 400 °C for 6 h. Filters were stored at -20 °C



247 before measurement. Samples were treated via fuming with 2N HCl to remove carbonates overnight and dried in the oven
248 for 4h. Finally, filters were folded into silver cups and stored in a desiccator until analysis. Samples were analysed for
249 carbon with a Thermo Finnigan EA 1112 Series Flash Elemental Analyser (CSL, University of Tasmania).

250

251 Biogenic silica (BSi) concentrations were analysed every 4 days by filtering 100 mL of seawater from each microcosm.
252 Mixed Cellulose Ester (MCE) membrane filters (diameter = 25 mm, pore size = 0.8 µm) were used for BSi samples. BSi
253 filters were placed in a plastic petri dish and stored at -20 °C before measurement. Filters were processed using the hot
254 NaOH digestion method of Nelson et al. (1989). The final solution was measured using the same process as the dissolved
255 silicate (see section 2.4).

256

257 A self-made plastic zooplankton net (20 mm height and 15 mm width) with a 210 µm mesh size was acid-washed first and
258 then used to collect zooplankton from microcosms before mineral addition on day 2, near the middle (day 13), and at the
259 end of the experiment (day 23). Samples were stored in 10 % formalin seawater solutions and kept at room temperature
260 until measurements. Zooplankton were quantified and identified under a Leica M165C microscope fitted with a Canon 5D
261 camera. The number of zooplankton from one mini-trawl in each collection was converted to the unit of individual L⁻¹ and
262 used for data analysis. The diversity of zooplankton communities was estimated with the Shannon Diversity Index (H)
263 calculated as:

264

$$265 \quad H = -\sum(pi \times \ln(pi)) \quad (6)$$

266

267 where pi is the proportion of the entire zooplankton community made up of individual species abundance, and ln is the
268 natural logarithm.

269

270

271 2.6 Statistic analysis

272 R studio was used for data analyses. Generalized additive models (GAMs) from the package “mgcv” were fitted to the data
273 to predict the changes over time. The GAMs all shared the same equations:

274

$$275 \quad Y = s(\text{Day}), \quad (7)$$

276

277 in which Y presents the dependent variable and s(Day) is the smooth term of the day of the experiment. Another GAM was
278 used to detect significant differences between treatments and the control:

279

$$280 \quad Y = s(\text{Day}) + s(\text{Day}, \text{by} = \text{oTreatment}) \quad (8)$$

281

282 In this equation, the variable “Treatment” includes three conditions: “Control”, “Slag” and “Olivine”; while “oTreatment”
283 is the ordered factor of the variable “Treatment” which allowed us to compare the GAMs smooth terms from different
284 treatments and the control (Simpson, 2017).

285



286 For the analysis of trace metal concentrations and zooplankton abundance, Generalized Linear Models (GLMs) from the
287 'stats' package were fitted to the data to determine significant differences between treatments and the control. The selection
288 of specific GLMs was based on the distribution of the raw data. One GLM equation is

$$289 \quad Y = Treatment + \frac{Day}{22} + \left(\frac{Day}{22}\right)^2 \quad (9)$$

291
292 with family = Gamma, where Y represents the measured parameter (abundance of a zooplankton species and dissolved
293 trace metal concentrations); treatment is the conditions (“Control”, “Slag” and “Olivine”); and Day represents the day of
294 the experiment. The other GLM equation,

$$295 \quad Y = Treatment + Day \quad (10)$$

297
298 with family = Gaussian, was employed for particulate trace metal data and the Shannon Diversity Index. To compare the
299 contribution of the three treatments on the measured parameters, Tukey's significant difference test was conducted on the
300 GLMs using the 'glht' function.

301

302 3. Results

303 3.1 Elemental composition and grain size of the finely-ground minerals

304 SEM analysis revealed the approximate elemental composition of olivine and slag powder (Table 1). Based on this analysis
305 the olivine composition resembles the Mg-rich olivine mineral “forsterite” (Mg_2SiO_4). The particle size spectrum of olivine
306 powder is shown in detail in Fig. S2. Roughly 69 % of the olivine particles, when measured by volume, fell within the
307 diameter range of 35 - 300 μm . Additionally, SEM analysis revealed high levels of Ca and O in the slag, indicative of the
308 considerable $Ca(OH)_2$ and CaO content of the powder (Table 1; please note that H cannot be measured with the applied
309 method). The particle size measurement (Fig. S2) showed that 78 % of the ground slag particles were between 35 - 300
310 μm .

311

312 **Table 1.** The weight percentage of elements from two minerals. Unit: wt %.

Element	O	Ca	Mn	Si	Mg	Fe	Al	Ti	Cr	Ni
Olivine	39.9	0.4		19.9	26.4	13.0	1.0			0.8
Steel slag	41.9	36.0	7.0	6.5	4.3	3.7	3.4	1.7	1.6	

313

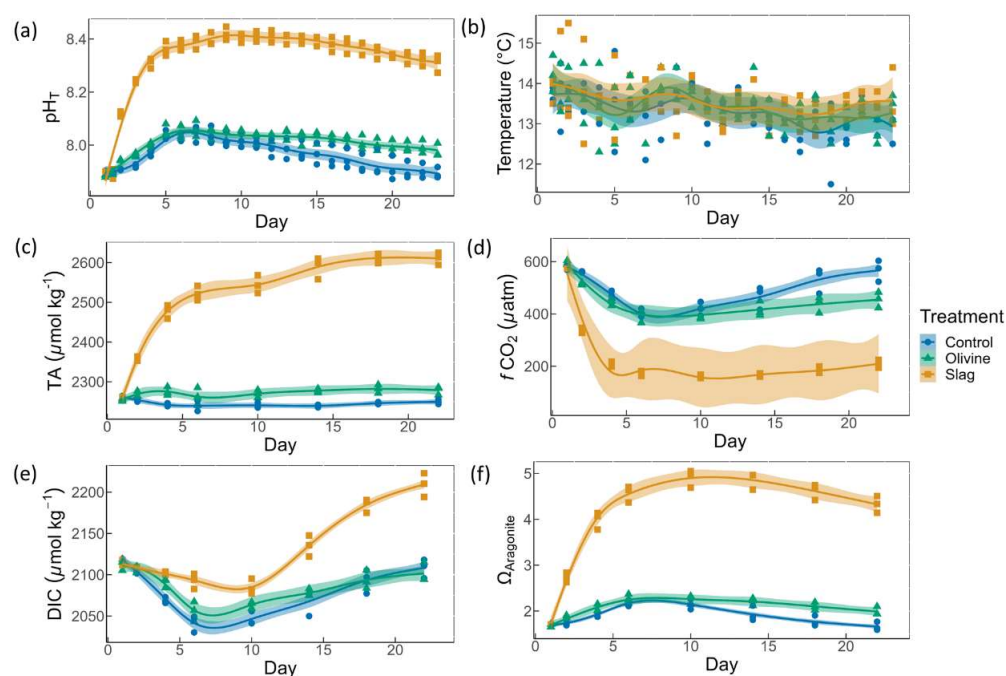
314

315 3.2 Physical and chemical conditions over the course of the experiment.

316 On day 2 of the experiment, when olivine particles were introduced into the microcosms, the smallest fraction of the powder
317 remained suspended, causing the seawater to become highly turbid for several days. The resulting milky appearance of the
318 seawater eventually faded over a period of approximately five days, and by day 5, the turbidity had visually become like



319 the slag treatment and the control. This effect was not anticipated, and as a result, we decided to investigate its impact on
320 light intensity. To do so, a test was conducted after the main experiment in which olivine powder was added to a microcosm
321 identical to those used in the experiment, and light intensity was measured daily at a depth of 0.15 m. The results showed
322 that the addition of olivine caused an initial reduction in light intensity of 18.5 % at 15 mins after addition, which declined
323 to 7.4 %, 3.7 %, 3.7 % and 0 % after 1, 2, 3, and 4 days, respectively. These findings indicate that olivine additions can
324 significantly affect the light environment in the microcosms, whereas no such effect was observed in the slag treatment.
325



326 **Fig. 2.** Carbonate chemistry conditions. The temporal development of (a) pH_T , (b) temperature, (c) total alkalinity (TA), (d) CO_2 fugacity
327 (f_{CO_2}) computed at *in situ* temperature and atmospheric pressure, (e) dissolved inorganic carbon (DIC), and (f) aragonite saturation state
328 ($\Omega_{\text{aragonite}}$). The dots represent the raw data ($n=3$ for each treatment per sampling time), and the fitted curve is the generalized additive
329 model (GAM). The shading represents the 95 % confidence interval of the fitted GAM.

331

332 The pH_T of all microcosms increased from day 1 to day 5 (Fig. 2a). This was partially due to photosynthetic CO_2 drawdown
333 during phytoplankton blooms that commenced in each microcosm. During the peak of the bloom, olivine addition led to a
334 slightly higher pH_T (8.054 ± 0.014 , average values \pm standard error) than the control (8.037 ± 0.010), but pH_T remained at
335 considerably higher levels in the olivine treatment after the bloom compared to the control. The slag addition increased the
336 pH_T in the microcosm from initially $7.897 (\pm 0.001)$ to $8.411 (\pm 0.015)$, which was significantly higher than the olivine
337 treatment and the control throughout the experiment. The final pH_T of the control, olivine, and slag treatments were 7.893
338 ± 0.012 , 7.978 ± 0.015 , and 8.309 ± 0.019 , respectively.

339

340 When comparing GAMs, P-means represent the p-value obtained from comparing two GAMs, such as the control and the
341 olivine treatment. If P-means is below 0.05, it indicates that the mean values of the two GAMs exhibit significant



342 differences over the course of the experiment. Conversely, if P-means is equal to or greater than 0.05, it suggests that the
343 two GAMs have similar mean values. In contrast, P-smooths represents the p-value derived from comparing the smooth
344 terms of two GAMs. If P-smooths is below 0.05, it indicates that the two GAMs demonstrate significantly different trends
345 in their change over time. In our analysis, all the fitted GAMs from the treatments and the control exhibited significant
346 differences in pH_T from each other, as evidenced by the p-values of both P-means and P-smooths being smaller than 0.001.
347 For detailed results of the GAM p-values, please refer to Table S1.

348

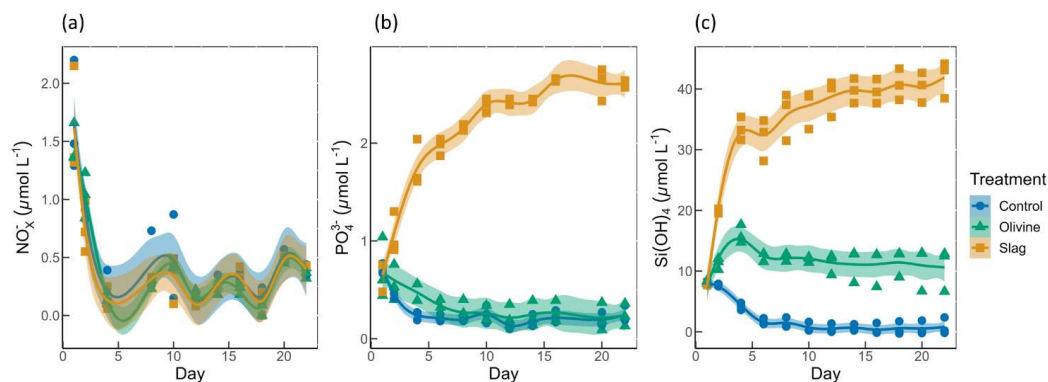
349 Total alkalinity increased marginally from 2255 ± 2 to $2262 \pm 13 \mu\text{mol kg}^{-1}$ within the first 6 days after olivine addition
350 while it increased more substantially from 2259 ± 1 to $2522 \pm 11 \mu\text{mol kg}^{-1}$ in the same time span in the slag treatment (Fig.
351 2c). The TA in the control decreased from $2261 \pm 2 \mu\text{mol kg}^{-1}$ to $2240 \pm 7 \mu\text{mol kg}^{-1}$ from day 1 to day 6 but remained
352 stable thereafter. The TA reached $2279 \pm 6 \mu\text{mol kg}^{-1}$ in the olivine treatment and $2611 \pm 9 \mu\text{mol kg}^{-1}$ in the slag treatment
353 group on day 22. The slag treatment reached a significantly higher TA than the olivine treatment and the control (P-
354 smooths < 0.001). The mean TA from GAM in olivine treatment was higher than the control group (P-means < 0.001).

355

356 The CO_2 fugacity ($f\text{CO}_2$) computed at *in situ* temperature and atmospheric pressure decreased continuously in the first 6
357 days in all microcosms (Fig. 2d). Then it increased again in the control and olivine treatments while staying lower in the
358 slag treatment. Dissolved inorganic carbon (Fig. 2e) and the aragonite saturation state ($\Omega_{\text{aragonite}}$; Fig. 2f) revealed a similar
359 trend over the course of the experiment in the control and the olivine treatment. In contrast, the slag treatment had higher
360 DIC and $\Omega_{\text{aragonite}}$ values throughout the experiment.

361

362



363

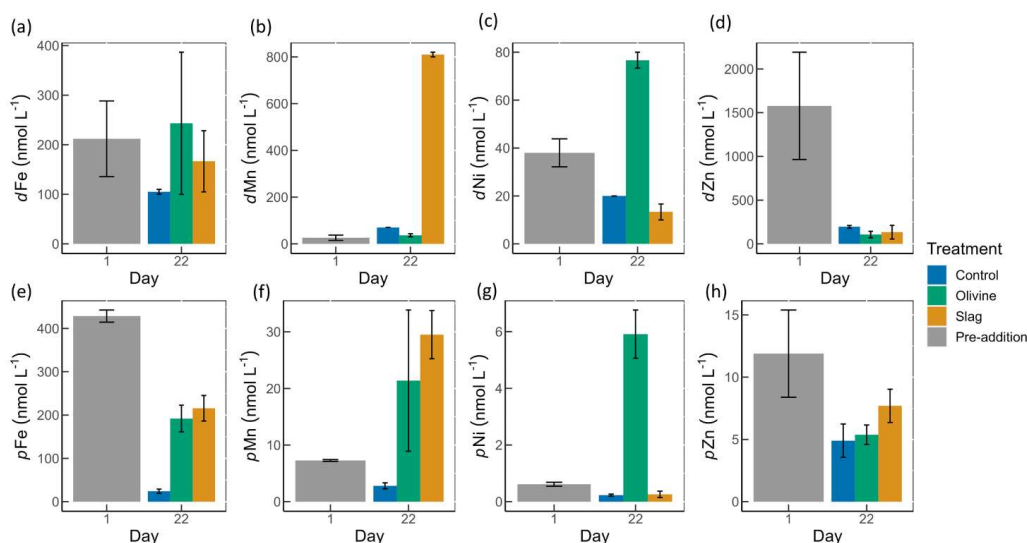
364 **Fig. 3.** Macronutrients concentrations over the course of the study. (a) Nitrate and nitrite concentrations. (b) Phosphate concentrations.
365 (c) Silicic acid concentrations. The dots represent the raw data ($n=3$ for each treatment per collection), and the fitted curve is the
366 generalized additive model.

367

368 Initial nitrate and nitrite (NO_x), phosphate (PO_4^{3-}), and silicic acid ($\text{Si}(\text{OH})_4$) concentrations were 1.58 ± 0.12 , 0.69 ± 0.59 ,
369 and $8.04 \pm 0.10 \mu\text{mol L}^{-1}$, respectively (Fig. 3). NO_x declined rapidly in all microcosms once the experiment had
370 commenced to values below $0.5 \mu\text{mol L}^{-1}$ and no significant difference was detected between treatments and control (P-
371 smooths > 0.05; Fig. 3a). In both the olivine treatment and the control, the PO_4^{3-} concentration decreased in the first six



372 days (Fig. 3b). In the slag treatment, PO_4^{3-} increased to a maximum of $2.65 \pm 0.01 \mu\text{mol L}^{-1}$, which was significantly higher
373 than in the olivine treatment and the control (P -means <0.001). The Si(OH)_4 concentration increased to a maximum of
374 $15.99 \pm 0.87 \mu\text{mol L}^{-1}$ in the olivine treatment, increased to a maximum of $41.92 \pm 1.75 \mu\text{mol L}^{-1}$ in the slag treatment, but
375 decreased below the detection limit in the control (Fig. 3c). Significant differences were observed in the development of
376 Si(OH)_4 between all treatments and the control (Table S1).
377



378
379 **Fig. 4.** Dissolved and particulate trace metal concentrations in microcosm seawater. (a)-(d) are dissolved trace metal concentrations, and
380 (e)-(h) are total particulate trace metal concentrations. The error bars represent the standard error from measured samples. The pre-
381 addition data shown in (a)-(d) represent the average of 5 microcosms before addition of slag or olivine. The data for the control on day
382 22 in (a)-(d) and for the pre-addition on day 1 in (e)-(h) were based on two of three microcosm replicates. The remaining data were based
383 on all three microcosm replicates.

384

385 After 21 days of experiment, the treatments showed a significant increase in dissolved Al concentrations from 504 ± 80 to
386 $970 \pm 228 \text{ nmol L}^{-1}$ in olivine treatment, and from 504 ± 80 to $1093 \pm 77 \text{ nmol L}^{-1}$ in slag treatment, while in the control
387 dissolved Al decreased to $230 \pm 10 \text{ nmol L}^{-1}$ (Fig. S3). The fitted GLMs were compared, and the p -value revealed how
388 much influence a treatment had on the dissolved metal concentrations (Table S2). The results indicate that the slag and
389 olivine additions led to significantly higher Al concentrations than in the control (p -values < 0.05), but no significant
390 difference was found between the two treatments (p -value = 0.189). The olivine treatment released Cu into the seawater,
391 and the Cu concentration in the olivine on day 22 was significantly higher than the slag treatment and the control (p -value
392 < 0.05) (Fig. S3). The addition of olivine and slag released some Fe, but overall, the concentration of Fe did not differ
393 between treatments (Fig. 4a). The slag released a substantial amount of dissolved Mn (maximum $820 \pm 10 \text{ nmol L}^{-1}$ on
394 day 22) (Fig. 4b), leading to significantly higher concentrations than in the olivine treatment and the control (p -values $<$
395 0.001). A significant amount of dissolved Ni was released from the olivine powder (p -values < 0.001) (Fig. 4c). The initial
396 concentration of dissolved Zn in seawater was much higher than on day 22 in all microcosms, and no significant difference



397 in Zn concentrations was found between the treatments and the control (Fig. S3).

398

399 Particulate concentrations of some trace metals also differed between treatments. The total particulate Fe decreased in all
400 microcosms on day 22 comparing with the pre-addition level, but both mineral addition treatments had higher particulate
401 Fe concentrations than the control on day 22 (Fig. 4e). The addition of slag elevated particulate Mn concentrations to a
402 level higher than the pre-addition and the control on day 22 (Fig. 4f), while the addition of olivine increased the particulate
403 Ni concentrations to a level higher than the slag, the control, and the pre-addition (Fig. 4g). The particulate Zn
404 concentrations in general decreased by the end of the experiment (Fig. 4h), and no significant differences were found
405 between the treatments and the control (Table S2).

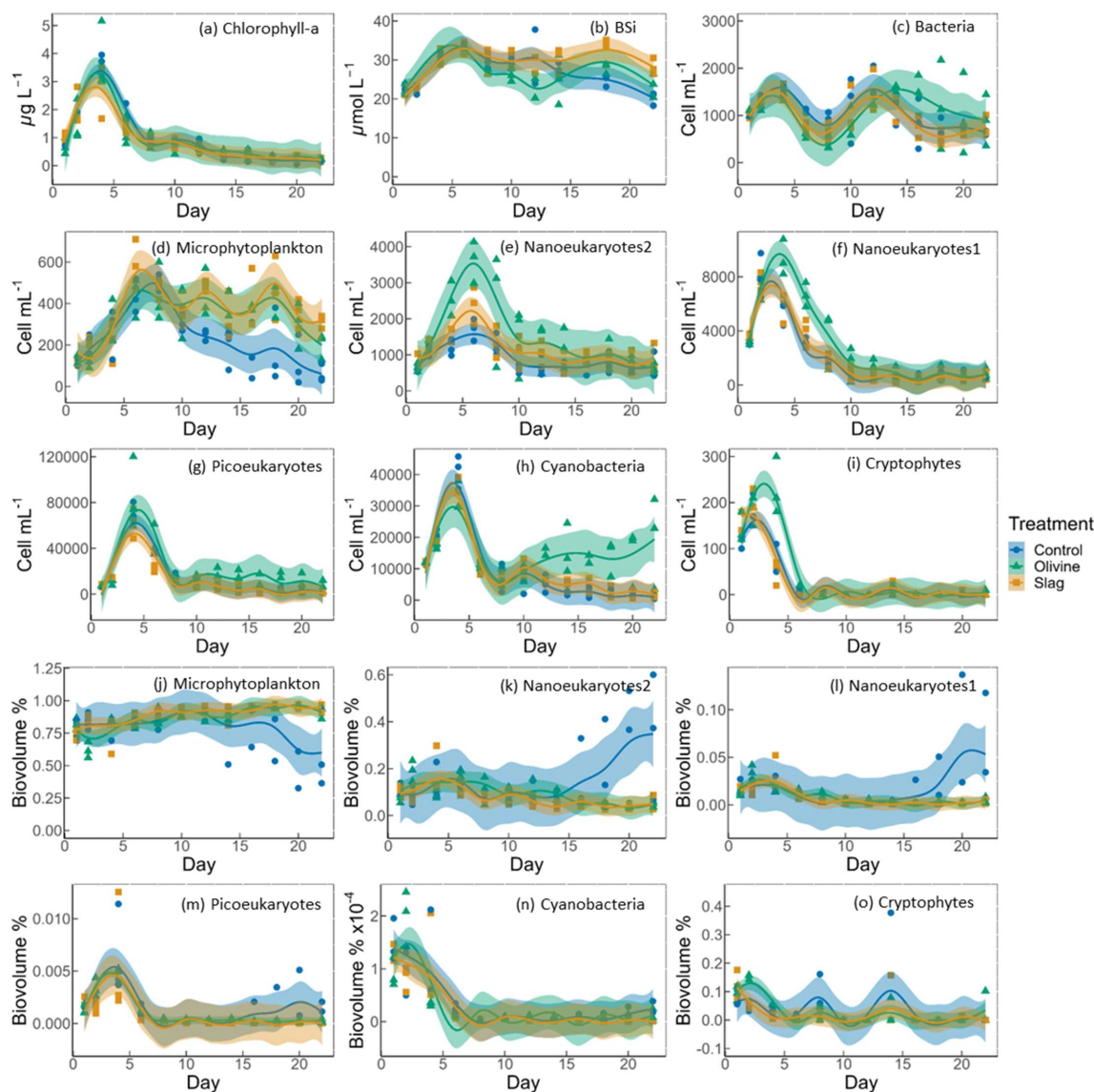
406

407 The POC on day 1 and day 22 from all microcosms were very similar, 10.99 ± 0.58 and $11.03 \pm 0.41 \mu\text{mol L}^{-1}$ respectively
408 (Fig. S4) so the metal:POC results were consistent with the particulate trace metal results (Fig. 4 e-h). In general, the non-
409 surface metal:POC are positively correlated with the total metal:POC ratios (Fig. S5). The ratio of non-surface to total
410 particulate trace metal concentrations is summarized in Table S4. Both non-surface and total Fe concentrations decreased
411 in microcosms on day 22 compared with the pre-addition level. Iron:POC ratios were significantly higher in the treatments
412 than in the control on day 22 (p-values <0.05 . Table S2), and there was no significant difference between mineral addition
413 treatments. The non-surface to total Fe:POC ratios were > 0.94 in all microcosms on both day 1 and day 22. The total and
414 non-surface Mn:POC ratio was the highest in the slag treatment. These ratios were higher than the pre-addition level and
415 the control at the end of the experiment. The total particulate Ni concentrations in the olivine treatment were significantly
416 higher than before olivine addition. The olivine treatment led to a >22 -fold higher Ni:POC ratio compared to the other two
417 treatments (p-value <0.001).

418



419 **3.3 Development and physiology of the plankton community**



420
 421 **Fig. 5.** Temporal development of chlorophyll-a concentration (chl-a), BSi, and different eukaryotic and bacterial plankton groups as
 422 determined with flow cytometry. (a) chlorophyll-a; (b) BSi; cell concentrations of (c) heterotrophic bacteria, (d) microphytoplankton, (e)
 423 nanoeukaryotes2, (f) nanoeukaryotes1 (g) picoeukaryotes, (h) cyanobacteria, and (i) cryptophytes; biovolume proportion of (j)
 424 microphytoplankton, (k) nanoeukaryotes2, (l) nanoeukaryotes1 (m) picoeukaryotes, (n) cyanobacteria, and (o) cryptophytes. The figure
 425 data points represent the raw data, and the fitted curve is the generalized additive model. The shaded area represents the 95 % confidence
 426 interval.

427

428 The chl-a concentration in all microcosms increased from day 1 to day 4 from $1 \mu\text{g L}^{-1}$ to $3\text{-}4 \mu\text{g L}^{-1}$ (Fig. 5a). The chl-a



429 concentration then decreased rapidly from day 4 to day 8, then continued to decrease, though more slowly, to $<0.3 \mu\text{g L}^{-1}$
430 until the end of the experiment. The GAMs of chl-a did not show any difference between treatments and the control (both
431 P-means and P-smooths >0.05 , see Table S1).

432

433 The BSi concentration increased from day 1 to day 6 in all microcosms (Fig. 5b). In the olivine and slag treatments, BSi
434 concentrations decreased slightly after the peak until day 12 but then increased again. In contrast, BSi concentration
435 decreased continuously in the control after the initial peak. Olivine particles suspended in seawater after the mineral
436 addition (see section 3.2) partially ended up on BSi filters during filtration. This led to extremely high BSi measurements
437 on days 2 and 4 that were removed from Fig. 5b. Without these outliers, the mean of fitted BSi GAM in the olivine treatment
438 was lower than the control and the slag treatment (Table S1), and the slag had the highest average BSi over the course of
439 the experiment. Overall, the BSi trends in the two treatments were similar (P-smooths = 0.269), although both were
440 significantly different from the control (P-smooths <0.05).

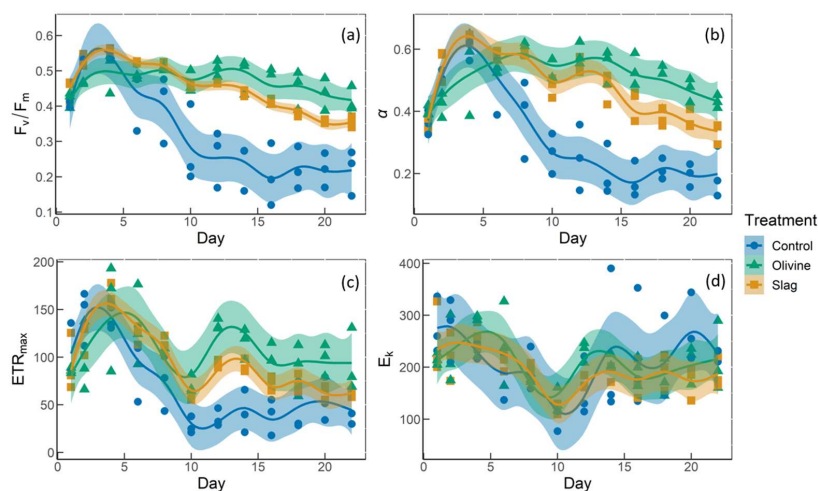
441

442 The development of the phytoplankton community composition showed significant differences between the treatments and
443 the control. In general, most phytoplankton groups exhibited similar patterns to chl-a, with peak cell numbers occurring on
444 day 4 (Fig. 5f-i). Following day 6, phytoplankton cell abundance generally decreased steadily. Microphytoplankton
445 displayed similar trends to the results for BSi. Before day 10, all microcosms had similar microphytoplankton abundances
446 (Fig. 5d). However, in the control group, microphytoplankton abundance declined continuously and at a faster rate
447 compared to the other two treatments (P-smooths values <0.03). From day 2 to day 6, the abundance of nanoeukaryotes1,
448 nanoeukaryotes2, picoeukaryotes, and cryptophytes was higher in the olivine treatment compared to the slag treatment and
449 the control. After day 8, their abundance decreased to a similar level as the other two groups. Notably, there were few
450 significant differences observed between the slag treatment and the control group in terms of the abundances of
451 nanoeukaryotes1, nanoeukaryotes2, picoeukaryotes, and cryptophytes throughout the experiment. In the olivine treatment,
452 cyanobacteria experienced a second bloom after day 10, which was significantly different from the other two groups (P-
453 smooths <0.01). Heterotrophic bacteria exhibited an increase and decline pattern following the phytoplankton bloom until
454 day 8 (Fig. 5c). Subsequently, bacteria abundance increased again, reaching a second peak during days 12-14, followed by
455 a decline until the end of the experiment. The decline in bacteria abundance was slower in the olivine treatment, although
456 no significant differences were detected between treatments (Table S1).

457

458 Among all the microcosms, microphytoplankton, nanoeukaryotes2, and cryptophytes consistently accounted for the largest
459 proportion of biovolume. From the perspective of biovolume proportion, the mineral addition mainly influenced the
460 microphytoplankton and nanoeukaryotes. The control had similar phytoplankton biovolume distribution as the treatments
461 from day 1 to day 15, but after that the proportion of microphytoplankton biovolume decreased to a level significantly
462 lower than the treatments. In the control treatment, the proportion of nanoeukaryotes' biovolume increased as the proportion
463 of microphytoplankton decreased. The biovolume of picoeukaryotes, cyanobacteria and cryptophytes increased during the
464 phytoplankton bloom and then decreased drastically after the bloom. There were no significant differences in biovolume
465 observed for picoeukaryotes, cyanobacteria and cryptophytes between the treatments and the control.

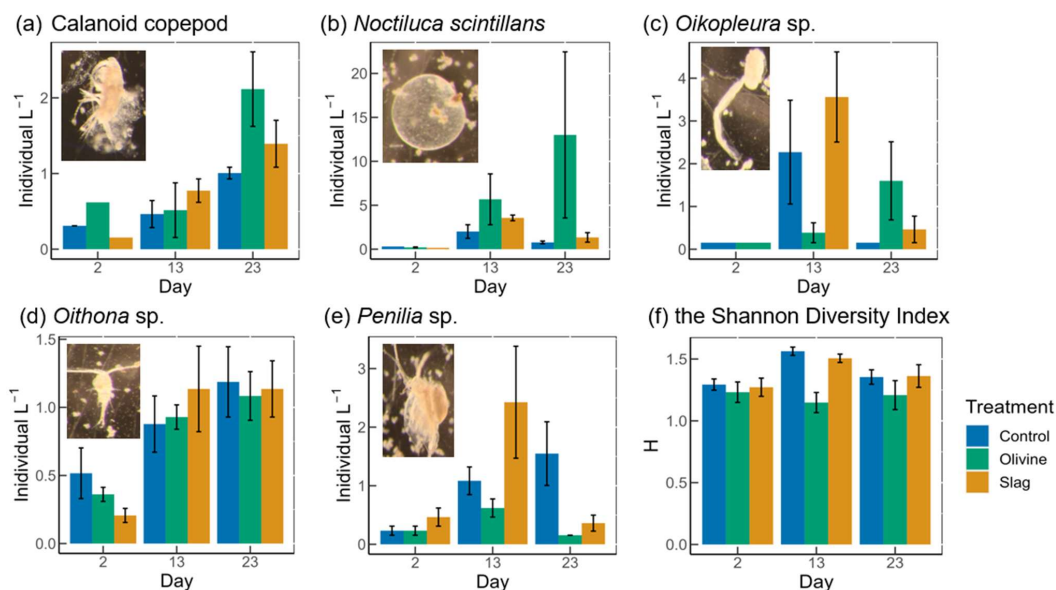
466



467
468 **Fig. 6.** The photosynthetic performance of the phytoplankton community. (a) F_v/F_m , the maximum quantum yield of photosynthesis II.
469 (b) α , the initial slope of the rapid light curves. (c) ETR_{max} is the maximum electron transport rate, the maximum potential photosynthetic
470 rate. (d) E_k is light-saturation parameter, Unit: $\mu\text{mol photons m}^{-2} \text{s}^{-1}$.
471

472 The temporal development of F_v/F_m , α , ETR_{max} , and E_k is illustrated in Fig. 6. The F_v/F_m values of the phytoplankton
473 community were approximately 0.42 ± 0.01 and increased to levels > 0.5 during the peak of the phytoplankton bloom
474 on day 4 (Fig. 6a). Following the bloom, F_v/F_m values dropped below 0.3 in the control. However, the decline in F_v/F_m after
475 the bloom was less pronounced in the two mineral addition treatments. At the end of the experiment, F_v/F_m was 0.22 ± 0.04
476 in the control, 0.35 ± 0.01 in the slag treatment, and 0.42 ± 0.02 in the olivine treatment. The temporal development of α
477 aligned with the patterns observed for F_v/F_m (compare Fig. 6a and 6b). The maximum values of ETR_{max} were observed on
478 day 4 in the control and the slag treatment, while in the olivine treatment, it occurred on day 5 (Fig. 6c). Subsequently,
479 ETR_{max} continuously decreased until day 10 and then stabilized until the end of the experiment. However, ETR_{max} exhibited
480 a subsequent increase in the mineral treatments around day 12. The ETR_{max} values were higher in the mineral treatments
481 compared to the control group (P-means < 0.001 , Table S1). The parameter E_k decreased from $246 \pm 17 \mu\text{mol photons m}^{-2}$
482 s^{-1} on day 1 to $121 \pm 7 \mu\text{mol photons m}^{-2} \text{s}^{-1}$ on day 10, and then it increased again to approximately $200 \mu\text{mol photons m}^{-2}$
483 s^{-1} by the end of the experiment (Fig. 6d). The change in E_k did not exhibit significant differences between the treatments
484 and the control (both P-means and P-smooths > 0.05).

485
486



487

488 **Fig. 7.** The dominant zooplankton abundance and community diversity from different treatments. Abundance of dominant zooplankton
489 in microcosms: (a) calanoid copepod; (b) *Noctiluca scintillans*; (c) *Oikopleura* sp.; (d) *Oithona* sp.; (e) *Penilia* sp.; and (f) the Shannon
490 diversity index (H) of different treatments and the control. Error bars represent the standard error calculated from three microcosm
491 replicates. Photographs of each zooplankton group are shown on the corresponding graphs.

492

493 Thirteen zooplankton taxonomic groups were identified in the microcosms. The dominant taxa were the appendicularian
494 *Oikopleura* sp., the cyclopoid copepod *Oithona* sp., the cladoceran *Penilia* sp., the heterotrophic dinoflagellate *N.*
495 *scintillans* and several calanoid copepods including *Acartia* sp., *Paracalanus* sp. and *Gladioferens* sp. The larvae and eggs
496 of *Oikopleura*, *Penilia* and copepod were also observed under the microscope. In general, higher zooplankton numbers
497 were observed after the bloom on day 13 (Fig. 7). The abundance of calanoid copepods and *Oithona* sp. increased after
498 day 2 (Fig. 7 a, d), and there was no significant difference between treatments and the control (p-values >0.05, Table S3).
499 The abundance of *N. scintillans* increased significantly more in the olivine treatment than in the control and the slag
500 treatment, with highest abundance of 13 ± 9 individual L^{-1} observed in the olivine treatment on the last day (Fig. 7 b). The
501 abundance of *Oikopleura* in the control and the slag treatment was higher than the olivine treatment on day 13 but was
502 higher in the olivine treatment on day 22 (Fig. 7c). A higher abundance of *Penilia* sp. was found in the slag treatment on
503 day 13 and in the control on day 23 (Fig. 7e). Due to the patchy distribution of zooplankton, these data have large standard
504 errors and only the differences in the numbers of *N. scintillans* in the olivine treatment were statistically significantly
505 different from the slag treatment and the control (p-value <0.05, Table S3).

506

507 Considering the control and slag treatment, the Shannon Diversity Index (H) increased from day 2 to day 13 and declined
508 on day 23, while in the olivine treatment, H was lower on day 13 than on day 2 and day 23 (Fig. 7f). The GLMs revealed
509 that the olivine treatment had significantly lower H on day 13 than the control and the slag treatment (p-values <0.001).
510 There were no significant differences in H between the control and the slag treatment (Table S3). The addition of olivine
511 decreased the zooplankton community's diversity. This is mainly driven by distinct trends observed in the abundance of
512 *Oikopleura* sp., *Penilia* sp., and *N. scintillans* (Fig. 7).



513

514 **4. Discussion**

515 **4.1 CO₂ removal potential of slag and olivine**

516 The slag powder created significantly higher CO₂ removal potential than the olivine powder over the course of the study.
517 Ca(OH)₂ and CaO in slag and Mg₂SiO₄ in olivine are likely to be the main functional minerals driving the measured
518 alkalinity enhancement. Total alkalinity increased by 361 μmol kg⁻¹ in the slag treatment while it increased by only 29
519 μmol kg⁻¹ in the olivine treatment, equivalent to a potential increase of the marine inorganic carbon by 14.7 and 0.9 %
520 within 3 weeks of their application. When normalizing these alkalinity increases to the same material weight, 1 g of slag
521 would release 9626 μmol TA while 1 g of olivine would release 16 μmol TA. Thus, over 3 weeks of experimental incubation,
522 slag is ~600-fold more efficient in releasing alkalinity for particles of this size class (please note that particle size spectra
523 of olivine and slag were similar but not identical; Fig. S1). We can also use these values to make a rough estimate of how
524 much CO₂ these two minerals could potentially sequester. One mole of alkalinity from olivine and slag can sequester
525 approximately 0.85 mole of CO₂. Thus, one tonne of slag and olivine powder as used here could sequester 360 and 0.6 kg,
526 respectively, within 3 weeks. It is likely that optimization of particle size and application method may lead to higher
527 efficiencies. Nevertheless, the slag showed potential as an OAE source mineral, even when applied as relatively coarse
528 powder in this experiment.

529

530 **4.2 OAE impacts on phytoplankton physiology and community**

531 The chlorophyll-a concentration was indistinguishable between treatments and the control suggesting a limited effect of
532 slag- or olivine-based OAE on phytoplankton bloom dynamics under these experimental settings. The phytoplankton
533 community was most likely N-limited after day 4 so that the release of Si(OH)₄ from olivine and Si(OH)₄ and PO₄³⁻ from
534 slag did not stimulate a further increase in chlorophyll-a concentration in the treatments. The development of BSi
535 concentrations is indicative of the prevalence of diatoms in the microcosms but differences between treatments and the
536 control were small. The release of Si(OH)₄ through olivine and slag will most likely benefit diatoms but this fertilization
537 effect did not manifest in this specific experiment because N was limiting diatom growth. However, when new N is supplied
538 then diatoms will likely take a bigger share of the limiting N pool when olivine or slag are used for OAE. As such, diatoms
539 are likely to benefit from olivine and slag applications, as has been shown in Si(OH)₄ manipulation experiments outside
540 the context of OAE research (Egge and Jacobsen, 1997). In the case of slag, the release of PO₄³⁻ will likely be another
541 driver that affects plankton productivity and community composition. As for Si(OH)₄, however, the effect of additional
542 PO₄³⁻ did likely not materialise in this experiment because PO₄³⁻ was not limiting over the course of the study. However, in
543 ecosystems where PO₄³⁻ is a limiting resource, the application of slag could enhance productivity with associated benefits
544 for higher trophic levels. In contrast, excessive applications of slag and concomitant PO₄³⁻ release could also pose a risk of
545 eutrophication. Future studies may need to investigate what the most sustainable dose of OAE via olivine and/or slag
546 applications could be.

547

548 The flow cytometry results further revealed the change in phytoplankton community composition. Both the olivine and



549 slag treatments sustained higher microphytoplankton abundances after the peak of the phytoplankton bloom on day 6. This
550 trend is consistent with some photophysiological parameters such as F_v/F_m so that it is tempting to assume that
551 photophysiological fitness gain measured with the FRRf led to higher competitiveness of microphytoplankton in the
552 community. Indeed, calculations of biovolume with flow cytometry data indicate that microphytoplankton were
553 predominantly contributing to the phytoplankton community biovolume so that the responses measured by the FRRf were
554 to a large extent driven by this group.

555

556 Apart from the increased microphytoplankton abundance, for the slag treatment, other phytoplankton groups distinguished
557 with flow cytometry did not deviate considerably from the control. The olivine addition, however, triggered more
558 pronounced shifts in the phytoplankton community. In particular, the nanoeukaryotes (roughly between 2-20 μm),
559 picoeukaryotes and the cryptophytes showed relatively higher abundance during the peak of the phytoplankton bloom, and
560 the abundance of cyanobacteria was higher after the bloom. We speculate that this shift following olivine treatment may
561 be attributable to a top-down effect from the decrease in zooplankton grazing effects in microcosms, which will be
562 discussed in section 4.3.

563

564 The measurement of photophysiological parameters revealed that the phytoplankton had generally better photosynthetic
565 performance in the slag and olivine treatments than in the control, especially after the phytoplankton bloom. During the
566 first 5 days, the changes in phytoplankton photosynthetic performance was indistinguishable amongst treatments. All
567 microcosms had similar health because of the relatively high NO_x^- concentrations and Fe supply (around 100 nmol L^{-1}).
568 After day 5, the F_v/F_m , α and ETR_{max} values decreased significantly faster in the control than in the treatments, and to values
569 lower than the initial condition. A decrease of F_v/F_m is commonly associated with physiological stress, such as nutrient
570 limitation, and high light stress (Bhagooli, et al. 2021), with Fe limitation causing a more pronounced decline in F_v/F_m than
571 nitrogen limitation (Gorbunov, et al 2021). ETR_{max} , which represents the maximum electron transport rate, has also been
572 shown to be negatively affected when phytoplankton experience nitrogen or Fe limitation (Kolber et al. 1994; Gorbunov
573 & Falkowski 2021). Furthermore, the change in photosynthesis performance after day 10 was suspected to be driven by
574 the microphytoplankton because the decrease of F_v/F_m , α , and ETR_{max} in the control was coupled with the decrease of
575 microphytoplankton abundance while the other phytoplankton groups were in low abundance as in the mineral addition
576 treatments, and the microphytoplankton contributed significantly (75 %) to community biovolume. All microcosms were
577 similarly NO_x^- limited from day 5 onward (Fig. 3) so that N-limitation is unlikely to explain different trends in
578 photophysiological parameters between the control and OAE treatments. Trace metals, especially Fe, released through slag
579 and olivine additions could potentially explain these differences.

580

581 Several of the trace metals released from slag and olivine are required for photosynthesis. For example, Fe is required for
582 many proteins functioning in photosynthesis, such as cytochromes, ferredoxin, and superoxide dismutase (SOD) (Twining
583 and Baines, 2013), and the addition of Fe can stimulate the growth of phytoplankton (Sunda and Huntsman, 1997) and
584 increase F_v/F_m (Behrenfeld et al., 2006). The dissolved and particulate Fe concentrations were higher in mineral addition
585 treatments than in the control indicating potentially more Fe available to sustain phytoplankton photosynthesis. While this
586 explanation is intriguing for the observed trends in photophysiology, it remains unclear why such strong differences
587 occurred between mineral addition and control treatments despite dissolved Fe concentrations of $\sim 100 \text{ nmol L}^{-1}$ at the end
588 of the experiment in the control. In Fe-limited ocean regions, dissolved Fe is at least two orders of magnitude lower, and



589 the enhancement of Fe to $\sim 1.5 \text{ nmol L}^{-1}$ can induce major phytoplankton blooms and relieve photophysiological stress (De
590 Baar et al., 2005). It is possible that these coastal phytoplankton species have higher Fe requirements than those from the
591 open ocean where Fe is limiting (Strzepek and Harrison, 2004). We speculate that when Fe was consumed during the
592 phytoplankton bloom, bioavailable Fe was much lower in the control, and may have been insufficient to meet the cellular
593 requirements of coastal phytoplankton. Our findings therefore suggest that Fe perturbations is not only relevant for lower
594 Fe open ocean regions but could also be relevant for coastal ocean locations.

595

596 Alternatively, the addition of Mn, Ni and other trace metals from mineral addition may have benefited photosynthesis.
597 Manganese is required for the water-splitting reaction of photosystem II (Armstrong, 2008), and both Mn and Ni are
598 common bioactive trace metals for SODs in marine phytoplankton. The noxious superoxide anion radical (O_2^-) generated
599 from aerobic respiration and oxygenic photosynthesis could be harmful to phytoplankton physiology, and SOD removes
600 O_2^- , thus improving photosynthesis (Wafar et al., 1995; Wolfe-Simon et al., 2005). This is consistent with our
601 photosynthetic measurements. Interestingly, although the amounts and types of trace metals released from the slag and
602 olivine powders were different, they led to relatively similar F_v/F_m values with only slightly higher F_v/F_m in the olivine
603 than the slag treatment from days 10-21. Over this time, these trace metal additions could have fertilized different
604 phytoplankton species because different phytoplankton could have different trace metal requirements, such as for SOD.
605 For example, cyanobacteria have NiSOD, diatoms have MnSOD, dinoflagellates have both FeSOD and MnSOD (Wolfe-
606 Simon et al., 2005). Another explanation is that phytoplankton in the control were limited by bicarbonate while the
607 treatments had sufficient bicarbonate from added minerals. However, we were unable to determine the species-level
608 changes in the phytoplankton community, and hence whether these trace metals, individually or combined, could account
609 for the observed phytoplankton community photosynthetic performance.

610

611 4.3 OAE impacts on the zooplankton community

612 Slag-based OAE did not significantly influence the zooplankton community composition while olivine-based OAE induced
613 some statistically significant effects, including a lower Shannon diversity. The increase in *N. scintillans* abundance and the
614 decrease in *Penilia* sp. and *Oikopleura* sp. in the olivine treatment indicate that the zooplankton response to OAE can vary
615 among different zooplankton types.

616

617 The observed lower abundance of *Oikopleura* sp. on day 13 in the olivine treatment may indicate a temporary suppression
618 or a slower growth rate of this zooplankton species in response to the olivine addition. This could be attributed to the
619 potential effects of olivine on the availability of essential nutrients or changes in the physicochemical environment of the
620 water. However, the subsequent increase in *Oikopleura* sp. abundance by day 22 suggests that the growth of this species
621 recovered or accelerated in the olivine treatment, leading to a higher abundance compared to the slag treatment and the
622 control on day 22. As discussed in section 4.2., reduced *Oikopleura* sp. abundance was unlikely due to reduced food
623 availability since phytoplankton within the preferred edible size spectrum, such as cyanobacteria and nanoeukaryotes, were
624 even more abundant in the olivine treatment. Instead, we hypothesize it to be an effect of the suspended olivine particles
625 that occurred for approximately the first 5 days of the study that were so plentiful that they turned the enclosed seawater
626 milky and may have clogged the mucous feeding mesh of *Oikopleura* sp (Lombard et al., 2011).

627



628

629 The abundance of *Penilia* sp. was lower in the olivine treatment than the other two groups throughout the experiment while
630 the abundance of *N. scintillans* was consistently higher. We cannot provide a particularly convincing hypothesis about
631 what specifically drove these differences though it is tempting to speculate that suspended particles present at the beginning
632 may have played a role also for those organisms since this was the only apparent systematic difference to the control and
633 slag treatment. The proliferation of *N. scintillans* can be problematic since heterotrophic dinoflagellate blooms can regulate
634 phytoplankton communities, cause toxicity to aquatic fish, and create an hypoxic sub-surface zone (Baliarsingh et al., 2016;
635 Zhang et al., 2020; Al-Azri et al., 2007), although a bloom of *N. scintillans* in southeast Australia only induced ichthyotoxicity
636 when the cell concentration reached 2,000,000 cells L⁻¹ (Hallegraeff et al., 2019). For comparison, we observed a maximum
637 of 32 cells L⁻¹ in one microcosm replicate of the olivine treatment.

638

639 In comparison to olivine, steel slag seemed to have less potential to affect zooplankton community composition. The
640 abundance of all groups of phytoplankton, apart from microphytoplankton after day 10, was similar in the slag treatment
641 and the control through the experiment. This is probably because the amount of slag powder added in the treatment was
642 much less than the olivine powder resulting in fewer physical particle perturbations to zooplankton. In addition, the
643 chemistry perturbations such as enhanced alkalinity concentration and various dissolved trace metals, especially Mn, from
644 the slag powder did not seem to have a notable direct influence on zooplankton abundance over the three-week period.
645 Even though we did not observe drastic zooplankton abundance changes during the experiment, considering there was
646 higher microphytoplankton abundance in the slag treatment after day 10, slag powder may benefit some zooplankton
647 especially those who feed on large phytoplankton on a longer time scale.

648

649 **4.4 Dissolved trace metal accumulation in seawater and its environmental implications**

650 The addition of olivine and slag as OAE source minerals released trace metals into the seawater, predominantly Al, Fe, Ni,
651 and Cu (olivine) as well as Al, Fe, and Mn (slag). The maximum measured concentrations for dissolved Al, Fe, Ni, Cu, and
652 Mn were 1190, 500, 80, 30, and 820 nmol L⁻¹, respectively. The threshold values for drinking water with health or aesthetic
653 considerations by the Australian Drinking Water Guidelines for Al, Fe, Ni, Cu, and Mn are 7400, 5360, 340, 15600, and
654 1800 nmol L⁻¹, respectively (NRMMC, 2022). All dissolved trace metal concentrations measured herein are well below
655 these health and aesthetic threshold values. In natural freshwater sources, the concentrations of Al, Fe, Ni, Cu and Mn are
656 generally less than 44000, 71400, 510, 156, and 25400 nmol L⁻¹ (NRMMC, 2022). Although these natural water data were
657 primarily derived from rivers and streams, they serve as valuable references for evaluating trace metal release in our
658 experiment. Thus, mineral additions to the microcosms as simulated here did not increase thresholds for any of the
659 measured trace metals beyond those that are considered safe for drinking water quality, and they were within the trace
660 metal concentration range in natural water. However, while these guidelines on drinking water provide a good starting point
661 on how to qualify what OAE perturbation could be considered “safe” and “unsafe” with regards to trace metals, it must be
662 recognized that seawater is not drinking water and that critical thresholds may be different in the latter.

663

664 The release of trace metals from OAE materials is considered to have relatively strong effects on biology, particularly in
665 the open ocean where trace metals usually occur in lower concentrations. For example, the oceanic Al, Fe, Ni, and Mn
666 concentrations are about 2, 0.5, 8, and 0.3 nmol L⁻¹ (Bruland and Lohan, 2003; Sohrin and Bruland, 2011). Previous



667 research on OAE-associated trace metal impacts on individual phytoplankton species grown in laboratory environments
668 has shown that concentration thresholds beyond which trace metal induces negative effects on fitness likely differ between
669 species (Guo et al., 2022; Hutchins et al., 2023; Xin et al., 2023). Indeed, our experiment with plankton communities
670 provides further support that several components of the planktonic food web are affected by OAE. However, our experiment
671 does not allow determining whether observed effects were primarily invoked by carbonate chemistry, macronutrient (P and
672 Si), or trace metal perturbations. Thus, dedicated experiments isolating the impact of these factors on plankton will be
673 required in the future.

674 **4.5 Particulate trace metal accumulation in seawater and its environmental implications**

675 The Derwent estuary (where we collected our plankton communities) was highly metal polluted due to industrial practice
676 (Macleod and Coughanowr, 2019). Both our dissolved and particulate trace metal data indicated high background metal
677 concentrations, especially for Fe and Zn. Furthermore, the metal:POC ratios found here (Fig. S5) are higher than reported
678 for open ocean studies or lab cultures. For example, the Fe:POC can vary from 2-136 $\mu\text{mol mol}^{-1}$ depending on the cultured
679 phytoplankton species and the environmental dissolved Fe concentration (Kulkarni et al., 2006; Sunda and Huntsman,
680 1995; King et al., 2012; Boyd et al., 2015). In our results the Fe:POC values ranged from 1200 to 39 000 $\mu\text{mol mol}^{-1}$, which
681 may be due to the particulate trace metal richness of the Derwent Estuary (control) and/or the addition of lithogenic particles
682 (slag and olivine treatment). The presence of abiotic particulate metal sources creates challenges to quantify metal quotas
683 and then to evaluate metal accumulation effects on biological organisms.

684

685 Our study reveals that the added minerals enriched the particulate trace metal pools to various degrees. Consistent with the
686 dissolved trace metal data, the slag treatment was enriched with particulate Fe and Mn while the olivine treatment was
687 enriched with particulate Fe and Ni. The enhanced particulate Ni and Mn concentrations were higher than before mineral
688 additions and the control levels. This is in line with previous research which indicates a positive correlation between
689 particulate and dissolved trace metal concentrations (Gaulier et al., 2019).

690

691 Based on the amounts released through OAE as simulated here (Fig. 4), it appears that Ni and Mn have the highest potential
692 to cause toxicity in certain marine organisms (Jakimska et al., 2011). These trace metals have the potential to accumulate
693 in marine organisms over time (bioaccumulation effects), and their increased concentrations in the food chain can lead to
694 adverse effects on the health and well-being of organisms at higher trophic levels (biomagnification effects). Previous
695 research has shown the bioaccumulation of Ni on zooplankton (Villagran et al., 2019; El-Metwally et al., 2022), oyster
696 (Chouvelon et al., 2022), molluscs (Andra Oros, 2010), and fish (Blewett and Wood, 2015); Mn in zooplankton (El-
697 Metwally et al., 2022), Antarctic bivalve (Husmann et al., 2012), clams (O'mara et al., 2019), and juvenile turbot (Van
698 Bussel et al., 2014). However, other studies revealed no biomagnification of Ni or Mn in the marine food webs (Sun et al.,
699 2020; Chouvelon et al., 2019; Campbell et al., 2005; Mathews and Fisher, 2008). Since it usually requires two connected
700 trophic levels be examined simultaneously (Colaço et al., 2006; Wang, 2002), it is hard to know whether the OAE-related
701 trace metal addition will be biomagnified. In addition, the bioaccumulation and biomagnification do not necessary result
702 in toxicity. Therefore, the next step is to investigate whether the enhanced dissolved/particulate trace metal will affect
703 higher trophic levels to estimate the environmental risks of OAE on other marine organisms.

704



705 **5 Conclusions**

706 Our study aimed to assess the environmental impacts of two ground OAE minerals, olivine and steel slag, on coastal
707 plankton communities. Both minerals released alkalinity, leading to an elevation in pH_T . However, the addition of steel
708 slag exhibited significantly higher efficiency in elevating alkalinity compared to olivine.

709

710 Overall, the application of olivine powder had a noticeable effect on the coastal plankton community. When comparing
711 this impact to the visible perturbation of the plankton community (the seawater turned highly turbid for about 4 days), the
712 impact appears to be modest. Under real-world conditions, dilution through physical mixing with unperturbed water would
713 further mitigate the perturbation. However, when comparing the impact on the plankton community to the limited alkalinity
714 enhancement and CO_2 removal potential that was achieved by adding $\sim 1.9 \text{ g L}^{-1}$ of olivine powder, it appears to be relatively
715 pronounced. While our experiment was only 3 weeks and olivine powder may slowly release more alkalinity, the short-
716 term response monitored here suggests that the immediate climatic benefit is relatively small compared to a relatively
717 pronounced environmental effect.

718

719 In general, the addition of steel slag powder had limited influence on both the phytoplankton and zooplankton community.
720 The major perturbations from slag powder are macronutrients (P and Si) and trace metal (Mn and Fe) additions. Although
721 limited environmental impacts were observed from the slag treatment in our experiment, if slag powders were applied at
722 large scale in the field, these perturbations may circulate in the ocean and influence plankton community well beyond the
723 experimental site. Furthermore, it is essential to consider that the composition of steel slag can vary depending on the
724 source factory (Wang et al., 2011; Proctor et al., 2000), which may affect the efficiency of carbon removal and change the
725 trace metal perturbation. Nevertheless, just based on our experiment, the comparison between the immediate climatic
726 benefit and environmental effect appears to be more favourable as for olivine.

727

728 Based on our findings, it can be concluded that steel slag powder exhibited fewer environmental impacts on plankton
729 communities compared to olivine powder, considering its capacity for alkalinity enhancement. The results highlight the
730 importance of carefully assessing the environmental consequences of using specific OAE minerals, particularly when
731 considering their potential effects on plankton communities.

732

733 **Data availability.** Data are available in the Institute for Marine and Antarctic Studies (IMAS) data catalogue, University
734 of Tasmania (UTAS) (<https://doi.org/10.25959/X6FH-9K15>, Guo, J., & Bach, L. (2023).).

735

736 **Author contributions.** LTB, RFS, KMS and JAG designed the experiments and JAG carried them out. LTB, RFS and
737 KMS supervised the study. ATT analysed the dissolved/particulate trace metal samples. JAG conducted statistical analyses.
738 JAG prepared the manuscript with contributions from all authors.

739

740 **Competing interests.** The contact author has declared that none of the authors has any competing interests.

741

742 **Disclaimer.** Publisher's note: Copernicus Publications remains neutral with regard to jurisdictional claims in published
743 maps and institutional affiliations.



744

745 **Acknowledgements.** We would like to thank Steve Van Orsouw from Moyne Shire Council, Victoria, Australia for
746 providing olivine rocks. We also thank Bradley Mansell who provided the Basic Oxygen Slag from Liberty Primary Steel
747 Whyalla Steelworks in Whyalla, South Australia, Australia. We appreciate Sandrin Feig and Thomas Rodemann for their
748 support on scanning electron microscopy, particle size measurement, and particulate organic matter. We appreciate the
749 assistance of Pam Quayle and Axel Durand (IMAS) in the lab, particularly with particulate metal digestions.

750

751 **Financial support.** This research has been supported by the Australian Research Council through a Future Fellowship
752 awarded to Lennart Thomas Bach (project FT200100846), and by the Australian Antarctic Program Partnership
753 (ASCI000002 to RFS, KMS and JAG). Access to SF-ICP-MS instrumentation was facilitated through ARC LIEF funding
754 (LE0989539) awarded to ATT.

755 References

- 756 Ackerman, L., Jelínek, E., Medaris, G., Ježek, J., Siebel, W., and Strnad, L.: Geochemistry of Fe-rich peridotites
757 and associated pyroxenites from Horní Bory, Bohemian Massif: Insights into subduction-related melt–rock reactions, *Chem.*
758 *Geol.*, 259, 152-167, <https://doi.org/10.1016/j.chemgeo.2008.10.042>, 2009.
- 759 Al-Azri, A., Al-Hashmi, K., Goes, J., Gomes, H., Rushdi, A. I., Al-Habsi, H., Al-Khusaibi, S., Al-Kindi, R., and
760 Al-Azri, N.: Seasonality of the bloom-forming heterotrophic dinoflagellate *Noctiluca scintillans* in the Gulf of Oman in
761 relation to environmental conditions, *Int. J. Oceans Oceanogr.*, 2, 51-60, 2007.
- 762 Andra Oros, M.-T. G.: Comparative data in the accumulation of five heavy metals (cadmium, chromium, copper,
763 nickel, lead) in some marine species (mollusks, fish) from the Romanian Sector of the Black Sea, *Recherches Marines*, 39,
764 89-108, 2010.
- 765 Armstrong, F. A.: Why did nature choose manganese to make oxygen?, *Philos. Trans. R. Soc. Lond. B Biol. Sci.*,
766 363, 1263-1270, <https://doi.org/10.1098/rstb.2007.2223>, 2008.
- 767 Bach, L. T., Gill, S. J., Rickaby, R. E. M., Gore, S., and Renforth, P.: CO₂ removal with enhanced weathering and
768 ocean alkalinity enhancement: potential risks and co-benefits for marine pelagic ecosystems, *Front. Clim.*, 1, 1-21,
769 <http://doi.org/10.3389/fclim.2019.00007>, 2019.
- 770 Baliarsingh, S. K., Lotliker, A. A., Trainer, V. L., Wells, M. L., Parida, C., Sahu, B. K., Srichandan, S., Sahoo, S.,
771 Sahu, K. C., and Kumar, T. S.: Environmental dynamics of red *Noctiluca scintillans* bloom in tropical coastal waters, *Mar.*
772 *Pollut. Bull.*, 111, 277-286, <https://doi.org/10.1016/j.marpolbul.2016.06.103>, 2016.
- 773 Basu, S. and Mackey, K. R. M.: Phytoplankton as key mediators of the biological carbon pump: their responses
774 to a changing climate, *Sustainability*, 10, 869, <https://doi.org/10.3390/su10030869>, 2018.
- 775 Behrenfeld, M. J., Worthington, K., Sherrell, R. M., Chavez, F. P., Strutton, P., McPhaden, M., and Shea, D. M.:
776 Controls on tropical Pacific Ocean productivity revealed through nutrient stress diagnostics, *Nature*, 442, 1025-1028,
777 <https://doi.org/10.1038/nature05083>, 2006.
- 778 Blewett, T. A. and Wood, C. M.: Salinity-dependent nickel accumulation and oxidative stress responses in the
779 euryhaline killifish (*Fundulus heteroclitus*), *Arch. Environ. Contam. Toxicol.*, 68, 382-394, [http://doi.org/10.1007/s00244-](http://doi.org/10.1007/s00244-014-0115-6)
780 [014-0115-6](http://doi.org/10.1007/s00244-014-0115-6), 2015.
- 781 Bowie, A. R., Townsend, A. T., Lannuzel, D., Remenyi, T. A., and van der Merwe, P.: Modern sampling and
782 analytical methods for the determination of trace elements in marine particulate material using magnetic sector inductively
783 coupled plasma-mass spectrometry, *Anal. Chim. Acta.*, 676, 15-27, <https://doi.org/10.1016/j.aca.2010.07.037>, 2010.
- 784 Boyd, P. W., Strzepek, R. F., Ellwood, M. J., Hutchins, D. A., Nodder, S. D., Twining, B. S., and Wilhelm, S. W.:
785 Why are biotic iron pools uniform across high- and low-iron pelagic ecosystems?, *Global Biogeochem. Cycles*, 29, 1028-
786 1043, <http://doi.org/10.1002/2014gb005014>, 2015.
- 787 Boyd, P. W., Jickells, T., Law, C., Blain, S., Boyle, E., Buesseler, K., Coale, K., Cullen, J., De Baar, H. J., and
788 Follows, M.: Mesoscale iron enrichment experiments 1993-2005: synthesis and future directions, *Science*, 315, 612-617,
789 <http://doi.org/10.1126/science.1131669>, 2007.
- 790 Bruland, K. W. and Lohan, M. C.: 6.02 Controls of Trace Metals in Seawater, in: *Treatise on Geochemistry*, edited
791 by: Elderfield, H., Holland, H. D., and Turekian, K. K., Elsevier Pergamon, 23-47, [http://doi.org/10.1016/b0-08-043751-](http://doi.org/10.1016/b0-08-043751-6/06105-3)
792 [6/06105-3](http://doi.org/10.1016/b0-08-043751-6/06105-3), 2003.
- 793 Burt, D. J., Fröb, F., and Ilyina, T.: The sensitivity of the marine carbonate system to regional ocean alkalinity
794 enhancement, *Front. Clim.*, 3, <http://doi.org/10.3389/fclim.2021.624075>, 2021.



- 795 Campbell, L. M., Norstrom, R. J., Hobson, K. A., Muir, D. C., Backus, S., and Fisk, A. T.: Mercury and other
796 trace elements in a pelagic Arctic marine food web (Northwater Polynya, Baffin Bay), *Sci. Total. Environ.*, 351-352, 247-
797 263, <http://doi.org/10.1016/j.scitotenv.2005.02.043>, 2005.
- 798 Caserini, S., Storni, N., and Grosso, M.: The availability of limestone and other raw materials for ocean alkalinity
799 enhancement, *Global Biogeochem. Cycles*, 36, <http://doi.org/10.1029/2021gb007246>, 2022.
- 800 Chouvelon, T., Strady, E., Harmelin-Vivien, M., Radakovitch, O., Brach-Papa, C., Crochet, S., Knoery, J., Rozuel,
801 E., Thomas, B., Tronczynski, J., and Chiffolleau, J. F.: Patterns of trace metal bioaccumulation and trophic transfer in a
802 phytoplankton-zooplankton-small pelagic fish marine food web, *Mar. Pollut. Bull.*, 146, 1013-1030,
803 <http://doi.org/10.1016/j.marpolbul.2019.07.047>, 2019.
- 804 Chouvelon, T., Auby, I., Mornet, L., Bruzac, S., Charlier, K., Araújo, D. F., Gonzalez, J.-L., Gonzalez, P., Gourves,
805 P.-Y., Méteigner, C., Perrière-Rumèbe, M., Rigouin, L., Rozuel, E., Savoye, N., Sireau, T., and Akcha, F.: Role of suspended
806 particulate material on growth and metal bioaccumulation in oysters (*Crassostrea gigas*) from a French coastal semi-
807 enclosed production area, Arcachon Bay, *J. Mar. Syst.*, 234, 103778, <https://doi.org/10.1016/j.jmarsys.2022.103778>, 2022.
- 808 Colaço, A., Bustamante, P., Fouquet, Y., Sarradin, P. M., and Serrão-Santos, R.: Bioaccumulation of Hg, Cu, and
809 Zn in the Azores triple junction hydrothermal vent fields food web, *Chemosphere*, 65, 2260-2267,
810 <http://doi.org/10.1016/j.chemosphere.2006.05.034>, 2006.
- 811 De Baar, H. J., Boyd, P. W., Coale, K. H., Landry, M. R., Tsuda, A., Assmy, P., Bakker, D. C., Bozec, Y., Barber,
812 R. T., and Brzezinski, M. A.: Synthesis of iron fertilization experiments: from the iron age in the age of enlightenment, *J.*
813 *Geophys. Res. Oceans.*, 110, <https://doi.org/10.1029/2004JC002601>, 2005.
- 814 Dickson, A. G., Sabine, C. L., and Christian, J. R.: Guide to best practices for ocean CO₂ measurements, North
815 Pacific Marine Science Organization, Canada2007.
- 816 Egge, J. and Jacobsen, A.: Influence of silicate on particulate carbon production in phytoplankton, *Mar. Ecol. Prog.*
817 *Ser.*, 147, 219-230, <http://doi.org/10.3354/meps147219>, 1997.
- 818 El-Metwally, M. E., Abu El-Regal, M. A., Abdelkader, A. I., and Sanad, E. F.: Heavy metal accumulation in
819 zooplankton and impact of water quality on its community structure, *Arab. J. Geosci.*, 15, 1-14,
820 <https://doi.org/10.1007/s12517-021-09424-x>, 2022.
- 821 Evans, C., O'Reilly, J. E., and Thomas, J.: A handbook for the measurement of chlorophyll and primary production,
822 1987.
- 823 Falkowski, P. G.: The role of phytoplankton photosynthesis in global biogeochemical cycles, *Photosynthesis*
824 *Research*, 39, 235-258, <https://doi.org/10.1007/BF00014586>, 1994.
- 825 Feng, E. Y., Koeve, W., Keller, D. P., and Oschlies, A.: Model-based assessment of the CO₂ sequestration potential
826 of coastal ocean alkalinization, *Earth's Future*, 5, 1252-1266, <http://doi.org/10.1002/2017ef000659>, 2017.
- 827 Ferderer, A., Chase, Z., Kennedy, F., Schulz, K. G., and Bach, L. T.: Assessing the influence of ocean alkalinity
828 enhancement on a coastal phytoplankton community, *Biogeosciences*, 19, 5375-5399, [http://doi.org/10.5194/bg-19-5375-](http://doi.org/10.5194/bg-19-5375-2022)
829 2022, 2022.
- 830 Package 'seacarb'-Seawater Carbonate Chemistry: <https://cran.r-project.org/web/packages/seacarb/index.html>,
831 last access: 2023/6/1.
- 832 Gaulier, C., Zhou, C., Guo, W., Bratkic, A., Superville, P. J., Billon, G., Baeyens, W., and Gao, Y.: Trace metal
833 speciation in North Sea coastal waters, *Sci. Total Environ.*, 692, 701-712, <http://doi.org/10.1016/j.scitotenv.2019.07.314>,
834 2019.
- 835 Guo, J., Bao, Y., and Wang, M.: Steel slag in China: Treatment, recycling, and management, *Waste Management*,
836 78, 318-330, <https://doi.org/10.1016/j.wasman.2018.04.045>, 2018.
- 837 Guo, J. A., Strzepek, R., Willis, A., Ferderer, A., and Bach, L. T.: Investigating the effect of nickel concentration
838 on phytoplankton growth to assess potential side-effects of ocean alkalinity enhancement, *Biogeosciences*, 19, 3683-3697,
839 <https://doi.org/10.5194/bg-19-3683-2022>, 2022.
- 840 Hallegraeff, G. M., Albinsson, M. E., Dowdney, J., Holmes, A. K., Mansour, M. P., and Seger, A.: Prey preference,
841 environmental tolerances and ichthyotoxicity by the red-tide dinoflagellate *Noctiluca scintillans* cultured from Tasmanian
842 waters, *J. Plankton Res.*, 41, 407-418, <https://doi.org/10.1093/plankt/fbz037>, 2019.
- 843 Hansen, H. P. and Koroleff, F.: Determination of nutrients, in: *Methods of seawater analysis*, edited by: Grasshoff,
844 K., Kremling, K., and Ehrhardt, M., 159-228, <https://doi.org/10.1002/9783527613984.ch10>, 1999.
- 845 Hartmann, J., West, A. J., Renforth, P., Köhler, P., De La Rocha, C. L., Wolf-Gladrow, D. A., Dürr, H. H., and
846 Scheffran, J.: Enhanced chemical weathering as a geoengineering strategy to reduce atmospheric carbon dioxide, supply
847 nutrients, and mitigate ocean acidification, *Rev. Geophys.*, 51, 113-149, <http://doi.org/10.1002/rog.20004>, 2013.
- 848 Humphreys, M. P., Lewis, E. R., Sharp, J. D., and Pierrot, D.: PyCO₂SYs v1. 8: marine carbonate system
849 calculations in Python, *Geosci Model Dev*, 15, 15-43, <https://doi.org/10.5194/gmd-15-15-2022>, 2022.
- 850 Husmann, G., Abele, D., Monien, D., Monien, P., Kriewis, M., and Philipp, E. E. R.: The influence of sedimentation
851 on metal accumulation and cellular oxidative stress markers in the Antarctic bivalve *Laternula elliptica*, *Estuar Coast Shelf*
852 *Sci.*, 111, 48-59, <http://doi.org/10.1016/j.ecss.2012.06.003>, 2012.
- 853 Hutchins, D. A., Fu, F.-X., Yang, S.-C., John, S. G., Romaniello, S. J., Andrews, M. G., and Walworth, N. G.:
854 Responses of globally important phytoplankton groups to olivine dissolution products and implications for carbon dioxide



- 855 removal via ocean alkalinity enhancement, bioRxiv [preprint], <https://doi.org/10.1101/2023.04.08.536121>, 2023.
- 856 Ilyina, T., Wolf-Gladrow, D., Munhoven, G., and Heinze, C.: Assessing the potential of calcium-based artificial
857 ocean alkalization to mitigate rising atmospheric CO₂ and ocean acidification, *Geophys. Res. Lett.*, 40, 5909-5914,
858 <https://doi.org/10.1002/2013GL057981>, 2013.
- 859 Jakimska, A., Konieczka, P., Skóra, K., and Namieśnik, J.: Bioaccumulation of metals in tissues of marine animals,
860 Part II: metal concentrations in animal tissues, *Pol J Environ Stud*, 20, 2011.
- 861 Keller, D. P., Feng, E. Y., and Oschlies, A.: Potential climate engineering effectiveness and side effects during a
862 high carbon dioxide-emission scenario, *Nat. Commun.*, 5, 3304, <https://doi.org/10.1038/ncomms4304>, 2014.
- 863 King, A. L., Sañudo-Wilhelmy, S. A., Boyd, P. W., Twining, B. S., Wilhelm, S. W., Breene, C., Ellwood, M. J.,
864 and Hutchins, D. A.: A comparison of biogenic iron quotas during a diatom spring bloom using multiple approaches,
865 *Biogeosciences*, 9, 667-687, <http://doi.org/10.5194/bg-9-667-2012>, 2012.
- 866 Kohler, P., Hartmann, J., and Wolf-Gladrow, D. A.: Geoengineering potential of artificially enhanced silicate
867 weathering of olivine, *Proc. Natl. Acad. Sci. USA*, 107, 20228-20233, <https://doi.org/10.1073/pnas.1000545107>, 2010.
- 868 Kourounis, S., Tsvivilis, S., Tsakiridis, P. E., Papadimitriou, G. D., and Tsiouki, Z.: Properties and hydration of
869 blended cements with steelmaking slag, *Cem. Concr. Res.*, 37, 815-822, <https://doi.org/10.1016/j.cemconres.2007.03.008>,
870 2007.
- 871 Kulkarni, P. P., She, Y. M., Smith, S. D., Roberts, E. A., and Sarkar, B.: Proteomics of metal transport and metal-
872 associated diseases, *Chemistry*, 12, 2410-2422, <http://doi.org/10.1002/chem.200500664>, 2006.
- 873 Lenton, A., Matear, R. J., Keller, D. P., Scott, V., and Vaughan, N. E.: Assessing carbon dioxide removal through
874 global and regional ocean alkalization under high and low emission pathways, *Earth. Syst. Dyn.*, 9, 339-357,
875 <https://doi.org/10.5194/esd-9-339-2018>, 2018.
- 876 Lombard, F., Selander, E., and Kiørboe, T.: Active prey rejection in the filter-feeding appendicularian *Oikopleura*
877 *dioica*, *Limnol. Oceanogr.*, 56, 1504-1512, <http://doi.org/10.4319/lo.2011.56.4.1504>, 2011.
- 878 Lueker, T. J., Dickson, A. G., and Keeling, C. D.: Ocean pCO₂ calculated from dissolved inorganic carbon,
879 alkalinity, and equations for K₁ and K₂: validation based on laboratory measurements of CO₂ in gas and seawater at
880 equilibrium, *Mar. Chem.*, 70, 105-119, [https://doi.org/10.1016/S0304-4203\(00\)00022-0](https://doi.org/10.1016/S0304-4203(00)00022-0), 2000.
- 881 Macleod, C. and Coughanowr, C.: Heavy metal pollution in the Derwent estuary: History, science and
882 management, *Reg. Stud. Mar. Sci.*, 32, <http://doi.org/10.1016/j.rsma.2019.100866>, 2019.
- 883 Mathews, T. and Fisher, N. S.: Trophic transfer of seven trace metals in a four-step marine food chain, *Mar. Ecol.*
884 *Prog. Ser.*, 367, 23-33, <http://doi.org/10.3354/meps07536>, 2008.
- 885 Moore, C. M., Mills, M. M., Arrigo, K. R., Berman-Frank, I., Bopp, L., Boyd, P. W., Galbraith, E. D., Geider, R.
886 J., Guieu, C., Jaccard, S. L., Jickells, T. D., La Roche, J., Lenton, T. M., Mahowald, N. M., Marañón, E., Marinov, I., Moore,
887 J. K., Nakatsuka, T., Oschlies, A., Saito, M. A., Thingstad, T. F., Tsuda, A., and Ulloa, O.: Processes and patterns of oceanic
888 nutrient limitation, *Nat. Geosci.*, 6, 701-710, <http://doi.org/10.1038/ngeo1765>, 2013.
- 889 Nelson, D. M., Smith Jr, W. O., Muench, R. D., Gordon, L. I., Sullivan, C. W., and Husby, D. M.: Particulate
890 matter and nutrient distributions in the ice-edge zone of the Weddell Sea: relationship to hydrography during late summer,
891 *Deep. Sea. Res. A*, 36, 191-209, [https://doi.org/10.1016/0198-0149\(89\)90133-7](https://doi.org/10.1016/0198-0149(89)90133-7), 1989.
- 892 Natural Resource Management Ministerial Council (NRMMC), Australian Government.: The Australian Drinking
893 Water Guidelines (2011) - Version 3.8 Updated 2022, <https://www.nhmrc.gov.au/about-us/publications/australian-drinking-water-guidelines#block-views-block-file-attachments-content-block-1>, 2022.
- 894 O'Mara, K., Adams, M., Burford, M. A., Fry, B., and Cresswell, T.: Uptake and accumulation of cadmium,
895 manganese and zinc by fisheries species: Trophic differences in sensitivity to environmental metal accumulation, *Sci. Total*
896 *Environ.*, 690, 867-877, <http://doi.org/10.1016/j.scitotenv.2019.07.016>, 2019.
- 898 Paquay, F. S. and Zeebe, R. E.: Assessing possible consequences of ocean liming on ocean pH, atmospheric CO₂
899 concentration and associated costs, *Int. J. Greenh. Gas Control.*, 17, 183-188, <https://doi.org/10.1016/j.ijggc.2013.05.005>,
900 2013.
- 901 Platt, T., Gallegos, C. L., and Harrison, W. G.: Photoinhibition of photosynthesis in natural assemblages of marine
902 phytoplankton, *J. Mar. Res.*, 38, 687-701, 1980.
- 903 Proctor, D. M., Fehling, K. A., Shay, E. C., Wittenborn, J. L., Green, J. J., Avent, C., Bigham, R. D., Connolly, M.,
904 Lee, B., Shepker, T. O., and Zak, M. A.: Physical and chemical characteristics of blast furnace, basic oxygen furnace, and
905 electric arc furnace steel industry slags, *Environ. Sci. Technol.*, 34, 1576-1582, <http://doi.org/10.1021/es9906002>, 2000.
- 906 Reichl, C., Schatz, M., and Zsak, G.: World mining data, 1-261, 2018.
- 907 Renforth, P.: The negative emission potential of alkaline materials, *Nat. Commun.*, 10,
908 <http://doi.org/10.1038/s41467-019-09475-5>, 2019.
- 909 Renforth, P. and Henderson, G.: Assessing ocean alkalinity for carbon sequestration, *Rev. Geophys.*, 55, 636-674,
910 <http://doi.org/10.1002/2016rg000533>, 2017.
- 911 Schallenberg, C., Strzepek, R. F., Schuback, N., Clementson, L. A., Boyd, P. W., and Trull, T. W.: Diel quenching
912 of Southern Ocean phytoplankton fluorescence is related to iron limitation, *Biogeosciences*, 17, 793-812,
913 <https://doi.org/10.5194/bg-17-793-2020>, 2020.
- 914 Schuiling, R. D. and Krijgsman, P.: Enhanced weathering: an effective and cheap tool to sequester CO₂, *Clim.*



- 915 Change, 74, 349-354, <https://doi.org/10.1007/s10584-005-3485-y>, 2006.
- 916 Selfe, C.: Developing Transfer Function to Measuring Phytoplankton Cellular Properties with Flow Cytometry,
917 Master's thesis, Institute of Marine and Antarctic Studies, University of Tasmania, Australia, 2022.
- 918 Simpson, G.: Comparing smooths in factor-smooth interactions II ordered factors:
919 <https://fromthebottomoftheheap.net/2017/12/14/difference-splines-ii/>, last access: March 2023.
- 920 Smith, S. M., Geden, O., Nemet, G. F., Gidden, M. J., Lamb, W. F., Powis, C., Bellamy, R., Callaghan, M. W.,
921 Cowie, A., Cox, E., Fuss, S., Gasser, T., Grassi, G., Greene, J., Lück, S., Mohan, A., Müller-Hansen, F., Peters, G. P.,
922 Pratama, Y., Repke, T., Riahi, K., Schenuit, F., Steinhäuser, J., Strefler, J., Valenzuela, J. M., and Minx, J. C.: The State of
923 Carbon Dioxide Removal - 1st Edition, <http://doi.org/10.17605/OSF.IO/W3B4Z>, 2023.
- 924 Sohrin, Y. and Bruland, K. W.: Global status of trace elements in the ocean, *TrAC, Trends Anal. Chem.*, 30, 1291-
925 1307, <https://doi.org/10.1016/j.trac.2011.03.006>, 2011.
- 926 Strzpek, R. F. and Harrison, P. J.: Photosynthetic architecture differs in coastal and oceanic diatoms, *Nature*, 431,
927 689-692, <http://doi.org/10.1038/nature02954>, 2004.
- 928 Su, B., Chen, Y., Guo, S., and Liu, J.: Origins of orogenic dunites: petrology, geochemistry, and implications,
929 *Gondwana Res.*, 29, 41-59, <https://doi.org/10.1016/j.gr.2015.08.001>, 2016.
- 930 Subhas, A. V., Marx, L., Reynolds, S., Flohr, A., Mawji, E. W., Brown, P. J., and Cael, B.: Microbial ecosystem
931 responses to alkalinity enhancement in the North Atlantic Subtropical Gyre, *Front Clim.*, 4,
932 <https://doi.org/10.3389/fclim.2022.784997>, 2022.
- 933 Sun, T., Wu, H., Wang, X., Ji, C., Shan, X., and Li, F.: Evaluation on the biomagnification or biodilution of trace
934 metals in global marine food webs by meta-analysis, *Environ. Pollut.*, 264, 113856,
935 <http://doi.org/10.1016/j.envpol.2019.113856>, 2020.
- 936 Sunda, W. G.: Trace metal-phytoplankton interactions in aquatic systems, in: *Environmental Microbe-Metal*
937 *Interactions*, edited by: Lovley, D. R., 79-107, <https://doi.org/10.1128/9781555818098.ch4>, 2000.
- 938 Sunda, W. G.: Feedback interactions between trace metal nutrients and phytoplankton in the ocean,
939 *Front. Microbiol.*, 3, 1-22, <http://doi.org/10.3389/fmicb.2012.00204>, 2012.
- 940 Sunda, W. G. and Huntsman, S. A.: Iron Uptake and Growth Limitation in Oceanic and Coastal Phytoplankton,
941 *Mar. Chem.*, 50, 189-206, Doi 10.1016/0304-4203(95)00035-P, 1995.
- 942 Sunda, W. G. and Huntsman, S. A.: Interrelated influence of iron, light and cell size on marine phytoplankton
943 growth, *Nature*, 390, 389-392, <http://doi.org/10.1038/37093>, 1997.
- 944 Tang, D. G. and Morel, F. M. M.: Distinguishing between cellular and Fe-oxide-associated trace elements in
945 phytoplankton, *Mar. Chem.*, 98, 18-30, <http://doi.org/10.1016/j.marchem.2005.06.003>, 2006.
- 946 Twining, B. S. and Baines, S. B.: The trace metal composition of marine phytoplankton, *Ann. Rev. Mar. Sci.*, 5,
947 191-215, <http://doi.org/10.1146/annurev-marine-121211-172322>, 2013.
- 948 van Bussel, C. G. J., Schroeder, J. P., Mahlmann, L., and Schulz, C.: Aquatic accumulation of dietary metals (Fe,
949 Zn, Cu, Co, Mn) in recirculating aquaculture systems (RAS) changes body composition but not performance and health of
950 juvenile turbot (*Psetta maxima*), *Aquacult. Eng.*, 61, 35-42, <https://doi.org/10.1016/j.aquaeng.2014.05.003>, 2014.
- 951 Villagran, D. M., Severini, M. D. F., Biancalana, F., Spetter, C. V., Fernandez, E. M., and Marcovecchio, J. E.:
952 Bioaccumulation of heavy metals in mesozooplankton from a human-impacted south western Atlantic estuary (Argentina),
953 *J. Mar. Res.*, 77, 217-241, <http://doi.org/10.1357/002224019826887362>, 2019.
- 954 Wafar, M., Le Corre, P., and L'Helguen, S.: *f*-Ratios calculated with and without urea uptake in nitrogen uptake
955 by phytoplankton, *Deep Sea Res. I Oceanogr. Res. Pap.*, 42, 1669-1674, [https://doi.org/10.1016/0967-0637\(95\)00066-F](https://doi.org/10.1016/0967-0637(95)00066-F),
956 1995.
- 957 Wang, Q., Yan, P., and Feng, J.: A discussion on improving hydration activity of steel slag by altering its mineral
958 compositions, *J. Hazard. Mater.*, 186, 1070-1075, <https://doi.org/10.1016/j.jhazmat.2010.11.109>, 2011.
- 959 Wang, W.: Interactions of trace metals and different marine food chains, *Mar. Ecol. Prog. Ser.*, 243, 295-309,
960 <http://doi.org/10.3354/meps243295>, 2002.
- 961 Wolfe-Simon, F., Grzebyk, D., Schofield, O., and Falkowski, P. G.: The role and evolution of superoxide
962 dismutases in algae, *J. Phycol.*, 41, 453-465, <https://doi.org/10.1111/j.1529-8817.2005.00086.x>, 2005.
- 963 Xin, X., Faucher, G., and Riebesell, U.: Phytoplankton response to Increased nickel in the context of ocean
964 alkalinity enhancement, *Biogeosciences* [preprint], <https://doi.org/10.5194/bg-2023-130>, 2023.
- 965 Zhang, W., Dong, Z., Zhang, C., Sun, X., Hou, C., Liu, Y., Wang, L., Ma, Y., and Zhao, J.: Effects of physical-
966 biochemical coupling processes on the *Noctiluca scintillans* and Mesodinium red tides in October 2019 in the Yantai
967 nearshore, China, *Mar. Pollut. Bull.*, 160, 111609, <https://doi.org/10.1016/j.marpolbul.2020.111609>, 2020.